Major Controls on Diagenesis in the Martin Bridge Formation:

Wallowa Mountains, Oregon

by

Jane Lyra Eisenberg

A thesis submitted in partial fulfillment of the
requirements for the degree of

Master of Science
in
Geology

Thesis Committee:
John Bershaw, Chair
Ashley Streig
Steven Bachtel

Portland State University
2021

Abstract

Diagenetic alteration in carbonates has long frustrated scientists who wish to use their chemistry and/or texture to understand conditions at the time of deposition. Though indicators of diagenesis are well documented, their interpretation is not always straightforward. Despite the large volume of research on the subject, the positive identification and interpretation of diagenesis is a source of ongoing debate in the scientific community.

The goal of this study is to better understand the timing of, and controls on, diagenetic alteration in the Martin Bridge Formation (MBF), a Triassic-aged limestone that was altered following deposition. Thirty-nine samples of MBF with differing textures and compositions were collected from the southern Wallowa Mountains (Oregon, USA). Of these, six samples were visually and geochemically characterized using stable ($\delta^{18}O$, $\delta^{13}C$) and clumped (Δ_{47}) isotope analysis. From these results, mineralizing fluid $\delta^{18}O$ values and W/R trajectories were estimated.

I interpret diagenetic alteration to have occurred in a primarily closed system, at W/R ratios ranging from 0.1 to 0.5 (average value ~0.3), by an initial fluid consistent with Mesozoic meteoric water ($\delta^{18}O$ = -3.8 to -6.5‰). My results suggest that depositional environment does not have a strong effect on alteration for MBF limestones. Rock texture does appear to have an effect on alteration, insofar as it influences original permeability, and therefore W/R ratio.

My results also place new constraints on the timing of diagenetic alteration in the MBF exposed in the southern Wallowa Mountains. Relatively high temperatures (99 - 245°C) constrained by my Δ_{47} results suggest that peak alteration occurred during emplacement of the Wallowa batholith in early Cretaceous time.

Acknowledgements

I am very lucky to have received a great deal of support and assistance throughout the process of writing this thesis.

First and foremost, I am deeply grateful for the support and expertise of my advisor Dr. John Bershaw. His openness, kindness and curiosity are inspirational, and without him this thesis would not have been possible.

My committee members, Dr. Ashley Streig and Dr. Steven Bachtel, have provided invaluable feedback and guidance. In particular, I'd like to thank Steve for his work in the field, as well as for giving me a phenomenal crash course in carbonate classification and stratigraphy.

The geochemistry work for this thesis was done in collaboration with Dr. Katherine Huntington and Andrew Schauer at the University of Washington's IsoLab. I am so grateful for their expertise and patience.

Dr. Leif Karlstrom, Dr. Kendra Murray, Dr. Marli Miller, and Christine Bachtel have all generously contributed maps, data, and discussions that have greatly enriched my work.

I am fortunate to have had the best field assistants in the world: Alex McLean, Elise Freeman, and my dad Len Eisenberg. Thank you for making the trek to the Wallowas to help me out.

My partner Tristan Pemble contributed to this thesis in innumerable ways, starting with agreeing to move to Portland so I could go to graduate school here in the first place. His

other contributions include but are not limited to: emotional support, figure wrangling, assistance with no less than 8 types of software, and making sure my devices were charged at all times in the field. Thank you so much.

Finally, I could not have completed this thesis without the support of my friends and family. In particular, I am deeply grateful to my parents for their unending love and support, and the members of S9 for making it a joy to come into the office every day.

Financial support for this research was provided by grants and scholarships from the Geological Society of America, the American Association of Petroleum Geologists / Northwest Energy Association, and Portland State University.

Contents

List of Tables

List of Figures

1.0 Introduction:

Diagenesis refers to a change in the mineralogical and textural properties of a rock or sediment at low (non-metamorphic) pressures and temperatures (James and Jones, 2016). In carbonates, diagenesis is a relevant topic because it affects key reservoir properties including porosity and permeability (Hiatt, 2000). An understanding of diagenesis is also critical to accurately interpreting paleoenvironmental information in carbonate rocks (Zachos et al., 1994; Garzione et al., 2004). Though indicators of diagenesis are well documented, their interpretation is not always straightforward. The positive identification and interpretation of diagenesis is a source of ongoing debate in the scientific community (Huntington and Lechler, 2015; Swart, 2015).

The Martin Bridge Formation (MBF) is a late-Triassic (Norian) carbonate platform which outcrops extensively in the Wallowa Mountains, northeast Oregon (Figure 1). Follo (1994), Whalen (1985, 1988), and Stanley et al., (2008) have studied the stratigraphy in depth, but comprehensive geochemical analyses have not been published. The MBF is an excellent candidate to study controls on diagenesis because it has been extensively, but unevenly, altered. Original textures and compositions are preserved to varying degrees throughout the geographical extent of the MBF (Follo, 1994).

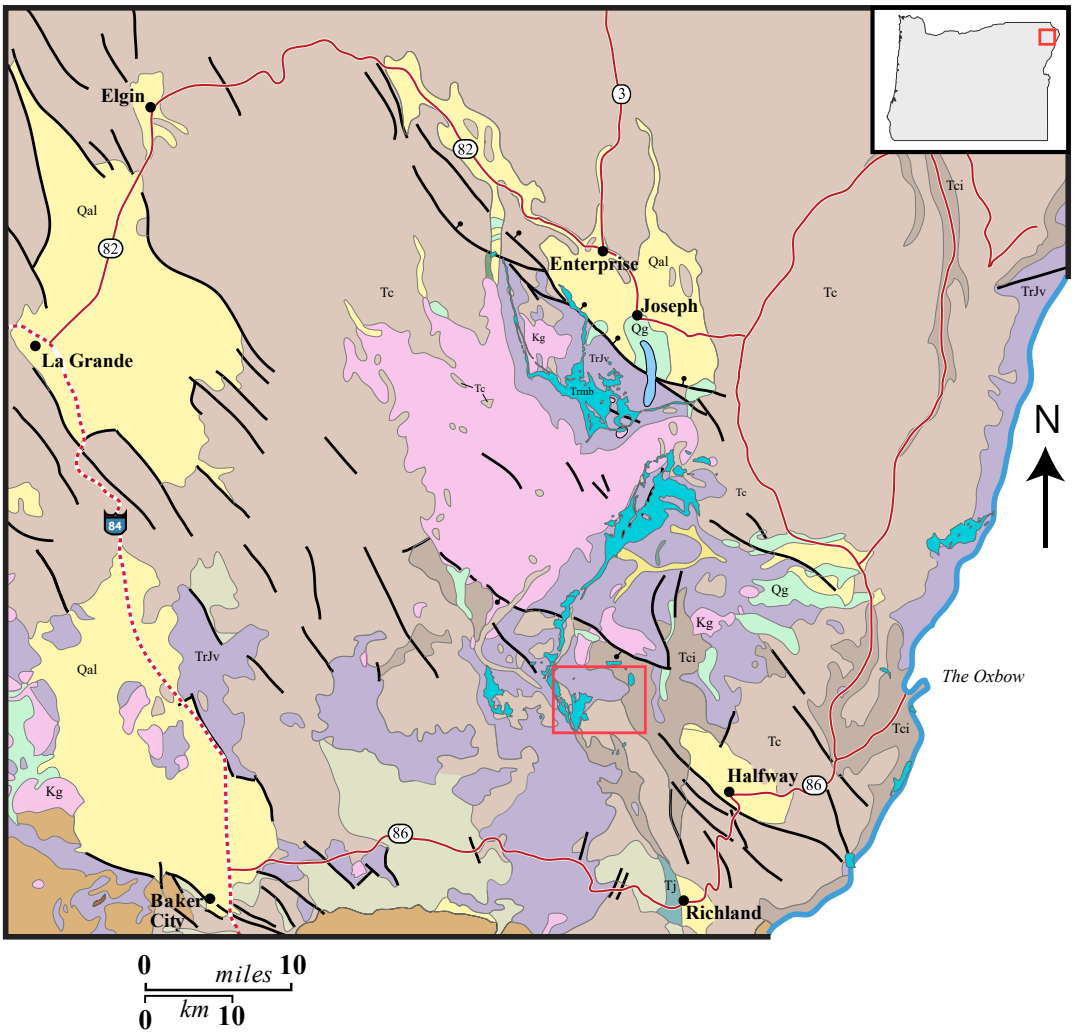

QUATERNARY

- Qal — Quaternary sediments, mostly alluvium.
- Qg — Quaternary glacial deposits.

TERTIARY

- Ts — Late Miocene-Pliocene sedimentary and volcanic rocks.
- Tc — Miocene CRBG, undifferentiated, but mostly Grande Ronde unit.
- Tci — Miocene Imnaha Basalt of the CRBG.
- Tj — Oligiocene John Day Formation.

INTRUSIVE ROCKS

- Kg — Jurassic-Cretaceous granitic rocks.

ROCKS OF ACCRETED TERRANE

- TrJb — Baker terrane: sedimentary and igneous rocks of a subduction complex.
- TrJw — Wallowa terrane: sedimentary and igneous rocks of an island arc.
- Trmb — Martin Bridge Formation limestones.

STRUCTURES

- Faults
- Normal faults

Figure 1: Simplified geologic map of the Wallowa Mountains, NE Oregon (see inset). Red box on the main map indicates the extent of Figure 3. Figure adapted from Miller (2014) using data from Walker and MacLeod (1991).

In addition to being an excellent target for diagenesis research, the MBF represents a uniquely preserved depositional environment. Unlike well-studied examples of late-Triassic reefs located in the European alps, the MBF is interpreted as a marginal reef where microbial fabrics and other small organisms were the primary reef builders (Martindale et al., 2012). Understanding the behavior of marginal reefs such as the MBF provides important insight into how modern reef trajectories may shift as climate change continues to impact their typical growth environments (Moura et al., 2016).

The goal of this study is to better understand the timing of, and controls on, diagenetic alteration in the MBF. In particular, this study investigates two of the major controls on diagenesis in the MBF: depositional environment and rock texture, and how they may have caused samples to experience variation in diagenetic alteration across outcrop to hand sample scales. The extent of diagenesis at two MBF localities is visually and geochemically characterized using petrographic, stable isotope, and clumped isotope analysis. The results of these analyses are considered in relation to carbonate texture, composition, depositional environment, and geographic location to interpret the timing and conditions of diagenetic alteration in the MBF, as well as identify the strongest controls on alteration in these samples.

2.0 Background

2.1 Wallowa Mountains

The Wallowa terrane is an intra-Panthalassic volcanic island arc that formed in late Paleozoic to early Mesozoic time. It is composed of volcaniclastic sediments and carbonates dating from the Permian – Triassic periods. The Wallowa terrane is interpreted to have collided with neighboring small island arc terranes in the mid to late Triassic. This string of amalgamated terranes then accreted to the North American craton by the end of the Jurassic period (Follo, 1994; Stanley et al., 2008; LaMaskin et al., 2015). Starting in the Jurassic period and continuing through the early Cretaceous, these sediments were intruded by granitic plutons which now form the Wallowa batholith (Follo, 1994; Johnson et al., 2011).

Following accretion, the Wallowa terrane was largely quiescent until the eruption of the first Columbia River Basalts (CRB) circa 16.7 ma. CRB stratigraphy suggests that the Wallowa terrane underwent modest subsidence immediately before the first eruptions, followed by ~2km of uplift between 15 Ma and 10 Ma (Hales et al., 2005). The modern Wallowa Mountains are predominantly covered by CRB, however the underlying terrane rocks are exposed in places due to erosion and deformation related to uplift.

2.2 Martin Bridge Formation

The MBF is a Norian aged limestone that outcrops sparingly in the Wallowa Mountains (Figure 1). It is comprised of limestones deposited on a shallow carbonate platform during a ~20 Ma quiescent period in Wallowa arc volcanism (Follo, 1994). Known exposures of the MBF represent two depositional environments: shallow platform (BC Creek and

Summit Point facies) and slope (Scotch Creek and Eagle Creek facies) (Stanley et al., 2008). Platform facies are dominated by carbonate sand shoals, with patches of coral, algal, microbial, and sponge reefs. The interior of the platform was comprised of protected evaporitic lagoons. Calcareous algae, sponge, spongimorph, coral, and bivalve fossils are all present in the platform facies, indicating a tropical locale at the time of deposition (Whalen, 1985; Follo, 1994). Paleomagnetic data suggest a 24 ± 12° N paleolatitude for the Wallowa terrane during the middle to late Triassic (Harbert et al., 1995).

The carbonate platform on which the MBF was deposited drowned in late Norian time (Follo, 1994). There are several feasible explanations for what might have triggered this drowning, the most obvious of which being sea level transgression (Whalen, 1988; Stanley et al., 2008). Dorsey and LaMaskin (2007) suggest that transgression was triggered by the incipient collision of the Wallowa terrane with an adjacent island arc, causing the development and migration of an outer flexural bulge throughout the basin. This was followed by deepening in the basin as an emergent thrust belt caused flexural subsidence. The transition from platform to deeper marine depositional environments is visible in the MBF as a deepening-upward succession throughout the Scotch Creek member. This succession eventually grades into the Hurwal Formation (HF), a deep water basinal facies composed of well lithified calcareous and non-calcareous argillites and fine-grained sandstone. Tuff, limestone, and conglomerate interbeds are common in the HF, and are thought to originate from island arc terranes to the north and south of the Wallowa terrane, as well as the Wallowa terrane itself (Follo, 1994).

Alteration is pervasive through the MBF and HF. However, the degree of alteration varies greatly with location. In general, exposures become more heavily recrystallized towards the north (Follo, 1994). Original depositional textures including bedding and fossils are preserved sparingly in the northern Wallowa Mountains, but are common throughout the southerly exposures. This study is focused in the southern Wallowa Mountains where original depositional textures have been more clearly preserved.

A detailed diagenetic history of MBF limestones exposed at Hells Canyon (BC Creek member) has been proposed by Whalen (1985), based on textural analysis. In brief, he proposes three main phases: (1) early diagenesis, (2) accretion-related regional neomorphism and structural deformation, and (3) intrusion-related local metamorphism. Hells Canyon is located ~50 km to the northeast of this study area, but Whalen's history has nonetheless been a useful framework for the interpretation of this study's data.

2.3 Stable Isotopes and Diagenesis

In this study, diagenesis of limestones is characterized using both visual and analytical means. Rock textures, such as cements and compaction features, are among the most widespread visual evidence used to interpret diagenesis (James and Jones, 2016). However, considerable uncertainty exists as a wide range of diagenetic processes may all result in similar textures.

Analytical means of characterizing diagenesis in carbonates such as stable isotopes ($\delta^{18}O$, $\delta^{13}C$, and Δ_{47}) are useful tools due to their ability to record the isotopic composition and temperature of the dominant diagenetic fluid. $\delta^{18}O$ and $\delta^{13}C$ values extracted from carbonate rocks are controlled by two factors: the $\delta^{18}O$ and $\delta^{13}C$ values of the dominant

fluid at the time the isotope values of the rocks were set, and the temperature at which setting occurred (James and Jones, 2016). $\delta^{18}O$ and $\delta^{13}C$ values that diverge from the baseline (seawater) fluid isotopic values can be correlated to changes in the diagenetic environment (Figure 2).

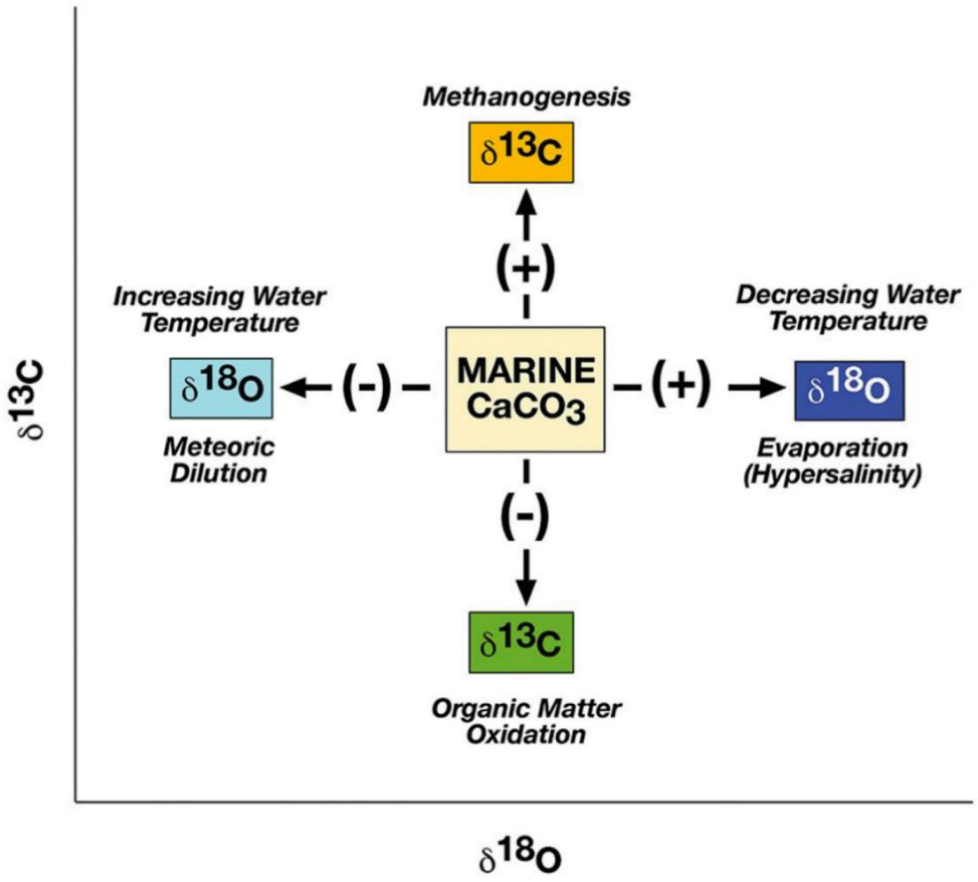

Figure 2: Schematic diagram of how changes in diagenetic environment may affect $\delta^{18}O$ and $\delta^{13}C$ values. Figure from James and Jones (2016).

Stable isotope ($\delta^{18}O$ and $\delta^{13}C$) analysis alone requires researchers to estimate the temperature of diagenetic fluid in order to obtain its $\delta^{18}O$ and $\delta^{13}C$ values. The addition of clumped isotope (Δ_{47}) analysis solves this problem by providing an independent estimate of mineralization temperature. The technique makes use of heavier isotopes' (^{13}C, ^{18}O)

tendency to bond with each other more readily at lower temperatures (Ghosh et al., 2006; Huntington and Lechler, 2015; James and Jones, 2016). In this study, both visual and analytical means of characterizing diagenesis are used to constrain the diagenetic environments preserved in the MBF.

3.0 Methods

3.1 Sample Selection

Two geographic areas in the southern Wallowa Mountains were selected for sampling based on previous workers' reports (Whalen, 1985; Follo, 1994; Stanley et al., 2008; Martindale et al., 2012) (Figure 3). Thirty-nine samples were collected from these locations in the summer of 2019 (Table 4, in Appendix). Samples were selected from each location

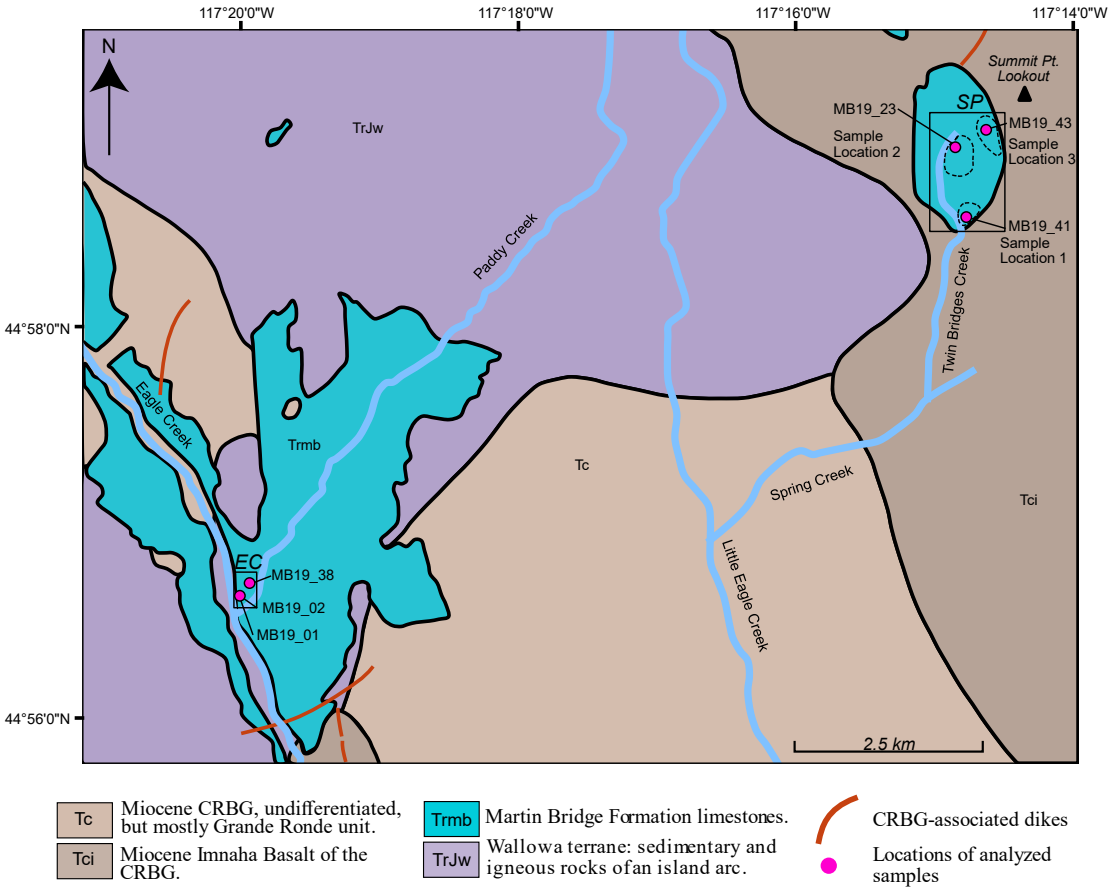

Figure 3: Simplified geologic map of the study locality. Boundaries between TrJw, Tc, and Tci are approximate and based on the work of Miller (2014). Trmb boundaries are based on geologic map data compiled by DOGAMI. Samples for this study were collected at Eagle Creek (EC) and Summit Point (SP) (Figures 4 and 10). Locations of analyzed samples are shown in magenta. The approximate extent of locations 1, 2, and 3 at SP (Figure 10) are shown by dashed lines within the SP locality. Note that at this scale, samples MB19_01 and MB19_02 (EC) overlie one another, and the low-angle fault described at EC is too small to be shown. Adapted from Miller (2014) using data from Walker and MacLeod (1991) and Morriss et al. (2020).

with a focus on obtaining a variety of depositional and secondary textures. In the lab, each sample was described and classified following the Dunham classification method (Dunham, 1962). Allochems were identified if present. Sample and outcrop descriptions, as well as interpretations by previous workers, were used to interpret the depositional environments represented by the samples.

3.2 Geochemistry

From the samples collected, thirteen representative samples from the southern Wallowa Mountains were initially selected for analysis. These samples represented the full breadth of Dunham classifications, and a variety of interpreted depositional environments. The carbonate percentages of each sample were determined by powdering ~1 gram of sample material using a ceramic mortar and pestle and dissolving the powder in 10% hydrochloric acid (HCl) over a period of ~24 hours. The remaining (non-carbonate) sediment was separated from the HCl using a vacuum pump, dried for 24 hours, and weighed. Carbonate percentages were calculated based on the difference in the weight of the original and remnant powders.

Samples with low (<70%) carbonate percentages were discarded, and spots of area ~0.25 cm^2 were selected for analysis on the remaining samples. The goal of spot selection was to sample the broadest range of textures and compositions that existed within each sample. A Dremel tool was used to grind off the outer ~1mm of rock to expose a fresh surface at each of the spots selected. Then, ~30 mg or more (depending on the carbonate percentage of the sample) of powder was drilled from each spot using the Dremel tool. Powders from 10 spots, representing 6 samples, were prepared with a custom vacuum line and analyzed for

$\delta^{18}O$, $\delta^{13}C$, and Δ_{47} on a Thermo MAT 253 at the University of Washington's IsoLab. For detailed analytical methods, refer to the Appendix.

3.3 Petrography

The six samples selected for isotope analysis were cut into thin sections and examined using transmitted and reflected light microscopy to further identify grain types and evidence of alteration in the samples.

3.4 Calculations

3.4.1 Fluid oxygen isotope composition

Fluid oxygen isotope compositions ($\delta^{18}O_w$) were calculated by applying temperatures yielded by clumped isotope data to the calcite-water fractionation equation of O'Neil et al. (1969). Refer to the Appendix for detailed calculations.

3.4.2 Water-Rock Modeling

The water-rock model developed by Banner and Hanson (1990) was utilized to understand how the isotopic compositions of both carbonate rock and fluid would evolve during closed-system diagenesis. The interpretation of closed-system behavior arises from the positive correlation between $\delta^{18}O_w$ and temperature (as explained in section 6.2.2). The model was generated using the following equations:

$$\delta_o = \frac{\left[\left(\delta_{(f,o)}\right)\left(C_{(f,o)}\right)F + \left(\delta_{(s,o)}\right)\left(C_{(s,o)}\right)(1-F)\right]}{C_o} \quad (1)$$

$$\delta_s = \frac{\left[\left(\delta_{o)}\right)(C_o)\left(\alpha_{(s-f)}\right) - 1000\left(C_f\right)F\left(1-\alpha_{(s-f)}\right)\right]}{\left[(C_s)(1-F)\left(\alpha_{(s-f)}\right) + C_f(F)\right]} \quad (2)$$

$$\delta_f = \frac{(\delta_s + 1000)}{\alpha_{s-f}} - 1000 \quad (3)$$

Where δ_o, δ_s, δ_f, $\delta_{f,o}$, and $\delta_{s,o}$ represent the oxygen isotopic composition of the total system, solid phase (calcite), fluid phase, initial fluid, and initial solid phase, respectively. $C_{f,o}$, $C_{s,,o}$, C_o, C_f, and C_s are the concentration of oxygen in the initial fluid, initial solid, total system (all phases), fluid, and solid. Following Loyd et al. (2015) I assume that $C_{f,o}$, = C_f, and $C_{s,,o}$, = C_s because the total oxygen concentrations of the different phases are not expected to change during alteration, only their isotopic compositions. *F* represents the weight fraction of fluid in the total system, and $\alpha_{s\text{-}f}$ refers to the equilibrium fractionation factor between solid and fluid in the system. Here, α is taken from the calcite-water fractionation equation of O'Neil et al. (1969). Specific input parameters can be found in Table 5 (Appendix).

4.0 Results

A total of 39 samples were analyzed through visual (macro and microscale) characterization. Six samples were selected for further geochemical analysis. The results of these analyses are presented here organized by analytical method.

4.1 Geochemistry

Table 1: Results of geochemical analyses for $\delta^{18}O$, $\delta^{13}C$, and Δ_{47}. EC = Eagle Creek, SP = Summit Point. Refer to Figure 3 for sample locations.

Sample Number	Area Sampled	Locality	$\delta^{13}C \pm 1$ SE (‰)	$\delta^{18}O \pm 1$ SE (‰)	$\delta^{18}O_w \pm 1$ SE (‰)	$\Delta_{47} \pm 1$ SE (°C)	Δ_{47} CDES Acid RF2 ± 1 SE (‰)
MB19_01_LOC1	dark laminae	EC	-1.40 ±0.01	-11.62 ±0.04	8.50 ±0.09	186 +40/-42	0.440 ±0.028
MB19_01_LOC2	light laminae	EC	-2.5 ±0.1	-11.54 ±0.07	9.57 ±0.15	204 +18/-16	0.426 ±0.012
MB19_02	brachiopod	EC	-0.625 ±0.005	-11.83 ±0.06	7.69 ±0.11	176 +16/-15	0.448 ±0.013
MB19_23_LOC1	oncoid layers	SP	1.68 ±0.03	-10.55 ±0.05	6.55 ±0.10	141 +12/-11	0.481 ±0.012
MB19_23_LOC2	oncoid core	SP	2.119 ±0.007	-7.54 ±0.05	10.96 ±0.10	160 +32/-26	0.462 ±0.027
MB19_23_LOC3	matrix surrounding oncoid	SP	3.159 ±0.005	-6.87 ±0.06	10.29 ±0.12	141 +15/-13	0.482 ±0.015
MB19_38	matrix	EC	-0.510 ±0.003	-10.27 ±0.02	12.74 ±0.03	245 +23/-21	0.401 ±0.012
MB19_41_LOC1	coral	SP	2.711 ±0.003	-6.86 ±0.04	11.35 ±0.07	155 +20/-17	0.467 ±0.018
MB19_41_LOC2	matrix	SP	2.71 ±0.04	-5.91 ±0.08	15.00 ±0.15	198 +27/-23	0.431 ±0.018
MB19_43	matrix	SP	4.034 ±0.002	-4.00 ±0.05	9.31 ±0.10	99 +14/-13	0.535 ±0.020

Geochemical analyses show a wide range of values in $\delta^{18}O$ (-11.83 — -4.00‰), $\delta^{13}C$ (-2.50 — 4.034‰), and Δ_{47} (0.401 — 0.535‰ / 99° – 245° C). When broken down by locality, samples from Eagle Creek (EC in Table 1) show higher average temperatures (average of 203° C) and more negative $\delta^{18}O$ and $\delta^{13}C$ values (averages of -11.32‰ and -1.25‰, respectively) than Summit Point. Samples from Summit Point show temperatures

with an average of 149° C and $\delta^{18}O$ and $\delta^{13}C$ values with averages of -6.97‰ and 2.74‰, respectively. Differences in temperature between EC and SP based on Δ_{47} data are within analytical uncertainty.

In three of the six samples, multiple spots were analyzed (MB19_01, MB19_23, and MB19_41). In all three of these samples, intrasample temperatures (Δ_{47}) were within standard error range of each other (about ±20° C). Intrasample oxygen isotope values ($\delta^{18}O$) were within standard error range of each other in sample MB19_01, and out of standard error range of each other in the other two samples (MB19_23 and MB19_41). Intrasample carbon isotope values ($\delta^{13}C$) were virtually identical to each other in sample MB19_41, but out of standard error range of each other in the other two samples (MB19_01 and MB19_23).

While Δ_{47} analysis is a source of potentially useful temperature information, it is subject to limitations and uncertainties (Huntington and Lechler, 2015). Of particular note in this study is the technique's lack of precision at high temperatures (Passey and Henkes, 2012). Large uncertainty ranges preclude confident interpretation of differences in temperature between samples.

4.2 Modeling

Temperature and oxygen isotope data ($\delta^{18}O_{carb}$ and $\delta^{18}O_w$) are plotted over closed-system evolution trajectories developed by Banner and Hanson (1990). The model allows for the generation of temperature-isotope trajectories for the evolution of carbonate minerals and fluids at variable water-rock (W/R) ratios. Similar approaches have been used by Loyd et al. (2015) and Huntington et al. (2011) to explore clumped isotope temperature and isotope

relationships of diagenetic calcites in limestones both (relatively) modern and ancient. The limestones in this study have ages between the limestones studied by Huntington (Eocene) and Loyd (Neoproterozoic).

5.0 Description and Interpretation of Samples and Locations

Samples from the southern Wallowa Mountains were collected from two localities: Eagle Creek and Summit Point (Figure 3). These locations are geographically close together, but contain diverse limestone types.

5.1 Eagle Creek

Eagle Creek is the type locality for the MBF (Stanley et al., 2008). The locality is comprised of one large section cross-cut by several small faults (McRoberts, 1990). For ease of description in this section, I have broken the rocks I observed at the Eagle Creek locality into five outcrops (Figure 4), which are described here along with their corresponding samples.

This section describes and interprets each outcrop / sample individually, then presents an overall interpretation for the locality.

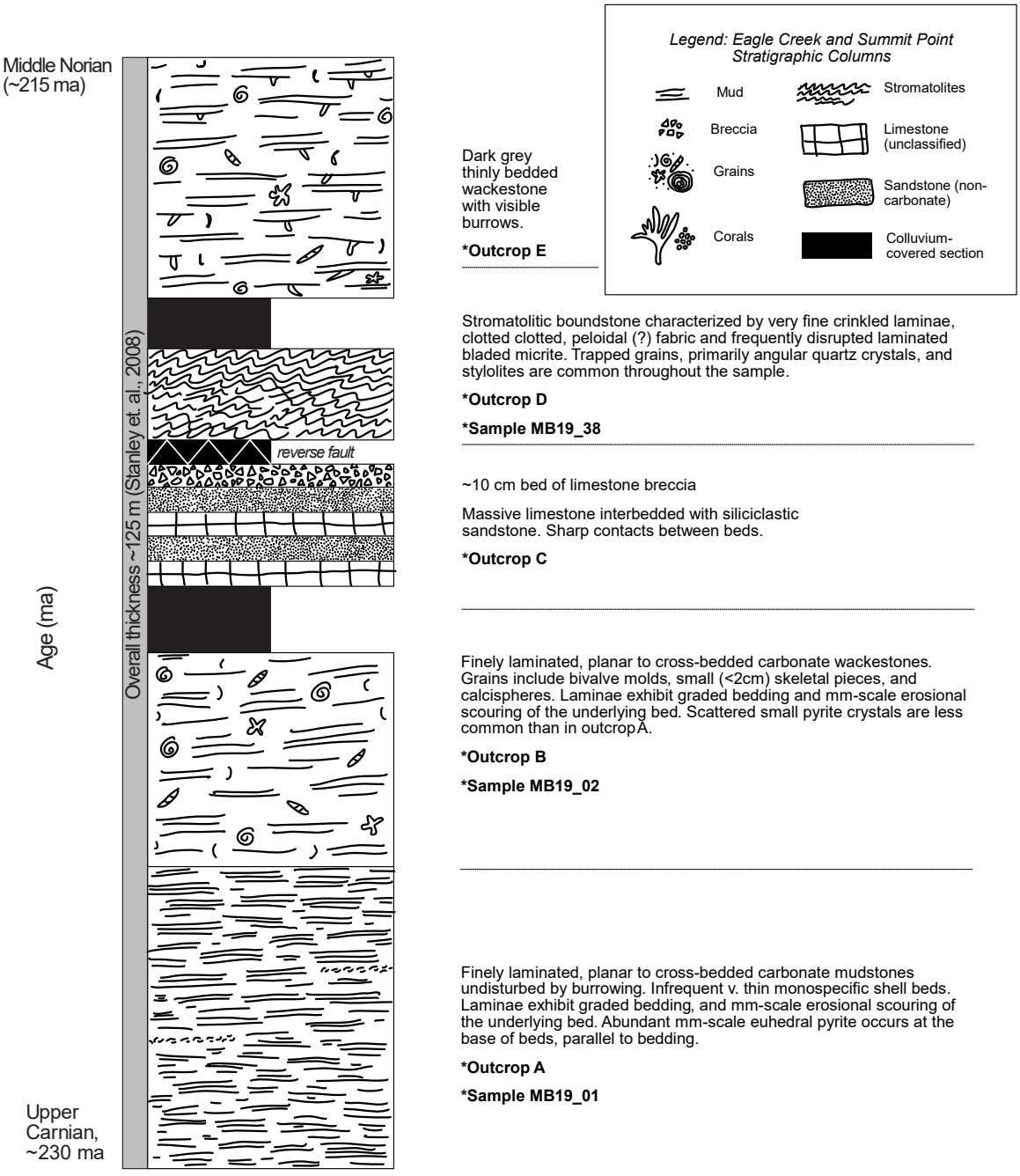

Figure 4: Stratigraphic column for the Eagle Creek section of the Martin Bridge Formation, Wallowa Mtns, OR. Thicknesses of individual units are approximate (not drawn to scale). Refer to Figure 3 for location map.

5.1.1 Outcrop A: Description

Outcrop A is comprised of finely laminated, planar to cross-bedded carbonate mudstones (Figure 5). The laminae alternate between light and dark grey in color. Light laminae tend to be coarser grained than dark laminae. The laminae are discontinuous on approximately a meter scale. Sedimentary structures include minor cross-beds, graded bedding, and mm-scale erosional scouring of the underlying bed. Abundant mm-scale euhedral pyrite occurs at the base of beds, parallel to bedding. No evidence of burrowing is visible.

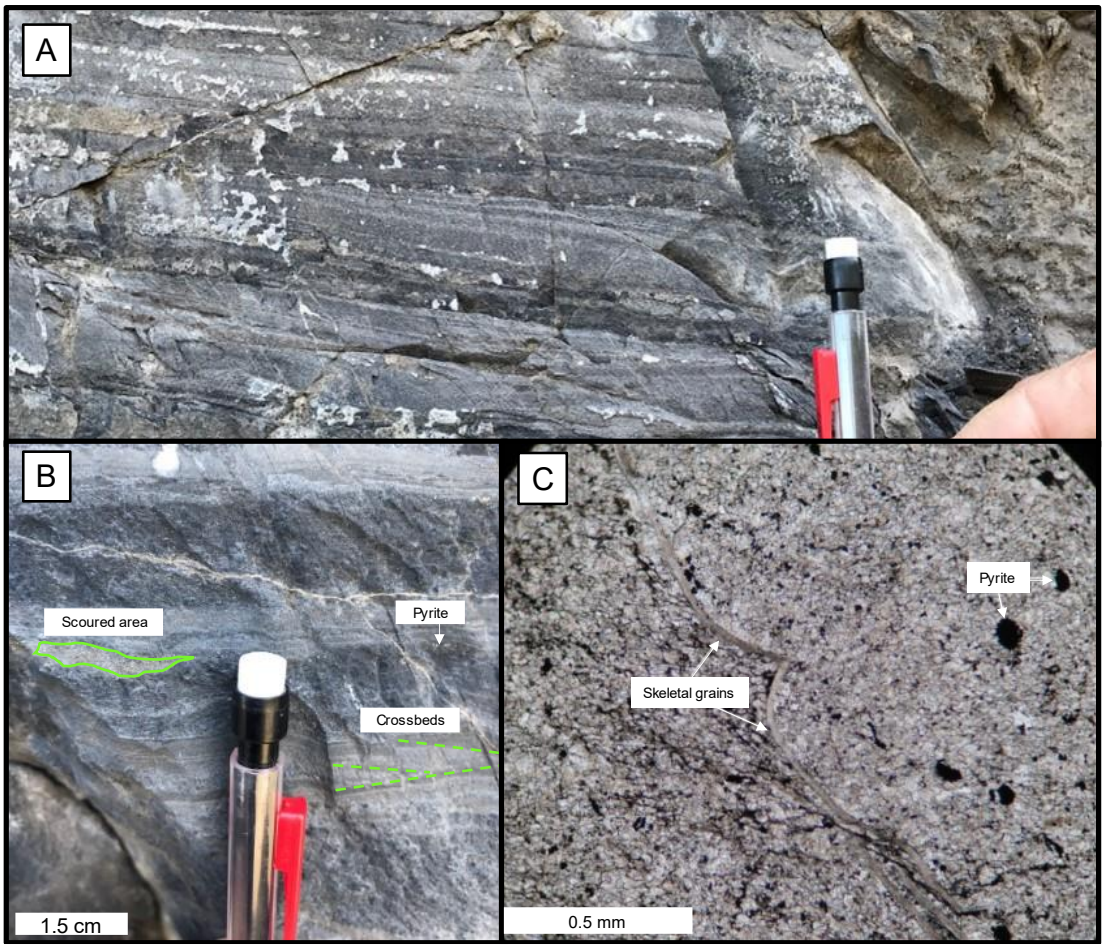

Figure 5: A) Laminated mudstones of outcrop A. Eraser tip of pencil measures 1.5 cm for scale. B) Closeup of outcrop A with bedding features labeled. C) Photomicrograph of sample MB19_01 taken in PPL showing the boundary between a dark laminae (SW) and a light laminae (NE). Distinctive grains are labeled.

Outcrop A is represented by sample MB19_01. Microscopy shows that MB19_01 is predominantly composed of 5-10 um subangular calcite grains. Opaque inclusions include pyrite and organic matter. Laminae are internally graded. In the dark-colored laminae, scattered monospecific skeletal pieces that appear to be shell edges are oriented parallel to bedding (Figure 5).

5.1.2 Outcrop A: Interpretation

Outcrop A is comprised of carbonate mudstone characterized by centimeter-scale laminae and fine grain size, indicating a slow, low-energy depositional process. Discontinuous laminae, channelization, and graded bedding indicate that deposition occurred via waxing and waning basinward flow, rather than sediment settling out of the water column. Abundant pyrite suggests an oxygen-poor environment at the time of deposition. The distinct laminae are undisturbed by burrowing features, further suggesting that fauna were scarce at the time of deposition. I interpret this outcrop to have been deposited in a calm, deep water environment on the distal slope of a carbonate platform.

5.1.3 Outcrop B: Description

Outcrop B is comprised of finely laminated, planar to cross-bedded carbonate wackestones. Although the rocks of outcrop B are primarily comprised of mud, brachiopod shell imprints and small (<2cm) unidentifiable skeletal grains are also visible in hand sample. The laminae alternate between light and dark grey in color, and light laminae still tend to be coarser grained than dark laminae. The laminae are discontinuous on approximately a meter scale, and, similarly to outcrop A, are interpreted to show evidence of waxing and waning flow through minor cross-beds, graded bedding, and mm-scale erosional scouring

of the underlying bed. No evidence of burrowing is visible. Pyrite is less common in outcrop B than in outcrop A, and where it does occur crystal sizes are smaller and less euhedral. Calcite cements occur in veins throughout the sample (Figure 6).

Outcrop B is represented by sample MB19_02, which is a wackestone containing multiple types of skeletal grains: brachiopods, round allochems interpreted as peloids, and abundant

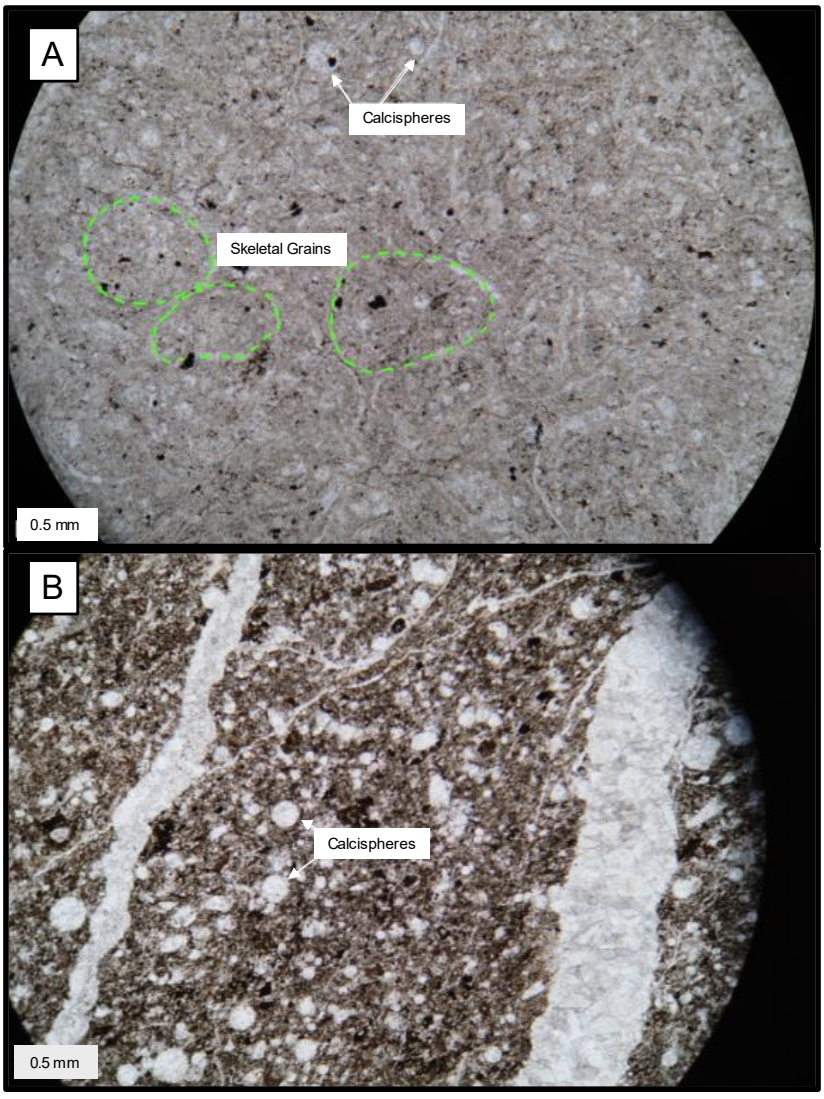

Figure 6:A) Photomicrograph of sample MB19_02 taken in PPL showing skeletal grains (traced in green) and calcispheres. B) Photomicrograph of sample MB19_02 taken in PPL showing distinct calcispheres. The darker groundmass in this photo is due to increased organic matter. The two thick veins crosscutting the sample are calcite and likely formed at a later date.

calcispheres. The groundmass is primarily calcite mud (~90%), with organic matter and quartz making up the remainder. Secondary calcite cement is apparent on the face of the sample, and fills multiple generations of veins up to 1mm in diameter throughout the sample. Opaques are mostly pyrite and altered pyrite (Figure 6).

5.1.4 Outcrop B: Interpretation

Bedding features, calcispheres (typically associated with deep water environments in Mesozoic time – Flügel (2010) and citations therein), and pyrite place this sample firmly in a deep water slope environment, while the increased amount of skeletal grains in MB19_02 indicate a more proximal environment relative to MB19_01.

5.1.5 Outcrop C: Description

Several meters of colluvial covered section separate outcrops B and C. At outcrop C, non-laminated planar limestone beds of medium thickness (~0.25 – 0.5 m) alternate with medium-thick non-calcareous sandstone beds (~0.5 m). Contacts between limestone and sandstone beds are sharp (Figure 7). A thin (~15 cm) breccia bed lies at the top of the section. The breccia is characterized by small (<3 cm) subangular limestone clasts. Above the breccia bed, the section is covered by colluvium. This colluvium-covered area contains a low-angle reverse fault mapped by McRoberts (1990). Below the fault, beds dip gently to the northeast, and above the fault they dip to the north. The stratigraphic displacement of this fault could not be determined in the field. While McRoberts (1990) does not specify displacement for individual faults in the area he mapped, he does note that stratigraphic displacement on thrust faults is typically only a few meters or less.

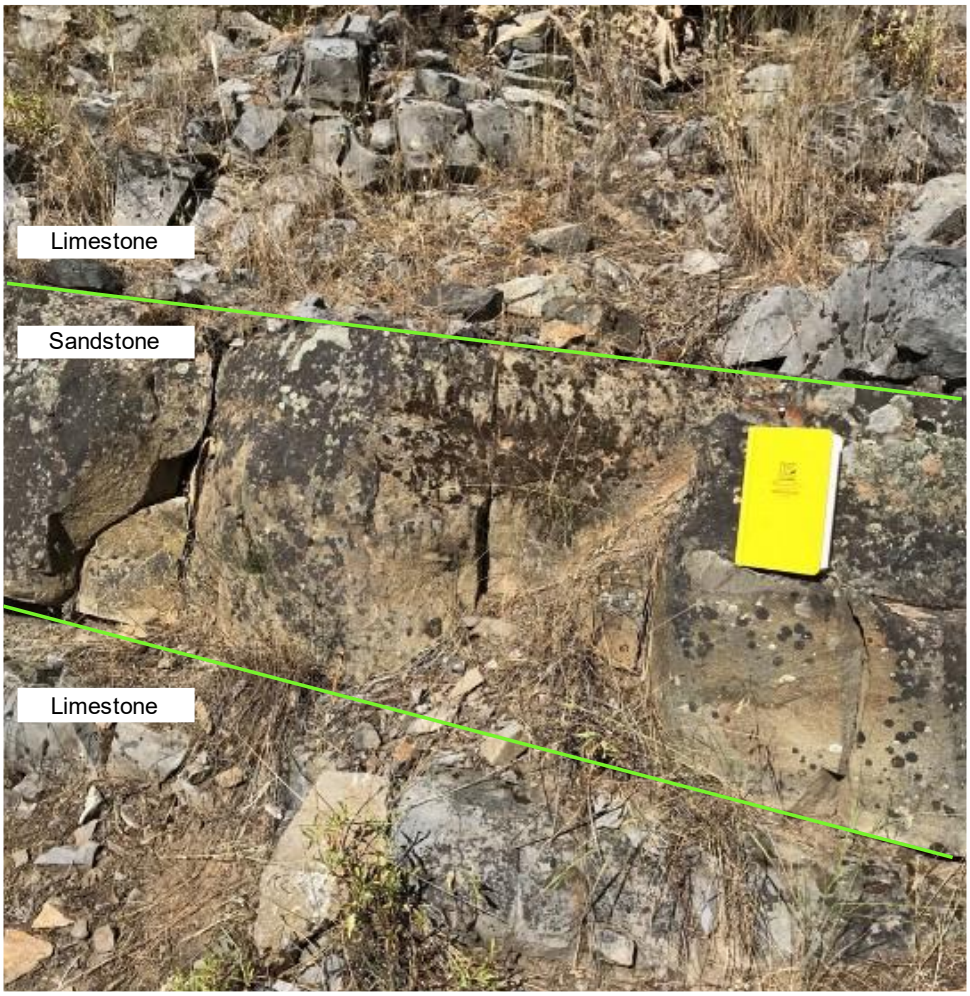

Figure 7: Field photo showing sharp contacts between limestone and sandstone beds at outcrop C. Yellow field notebook measures 19 cm for scale.

5.1.6 Outcrop C: Interpretation

I interpret outcrop C to represent a drop in sea level, resulting in the encroachment of fluvial systems on to the slope. The thin breccia bed at the top of this section could be (1) an indicator of sub-aerial exposure or (2) a collapse breccia triggered by the rapid sea level fall. Because of the small degree of displacement likely caused by the fault in this section, I contend that outcrop D is likely stratigraphically above outcrop C, and have treated it as such throughout my interpretations (Figure 4).

5.1.7 Outcrop D: Description

Outcrop D is separated from outcrop C by ~5 m of colluvial covered section containing a low-angle, small displacement reverse fault, as mapped by McRoberts (1990). Outcrop D consists of an ~0.5 m thick bed of limestone characterized by very fine crinkled laminae (Figure 8). A thin (~1cm) brachiopod shell bed is visible at the base of the outcrop.

Outcrop D is represented by sample MB19_38. Thin section analysis of sample MB19_38 shows that the sample is comprised of two dominant textures: clotted peloidal fabrics

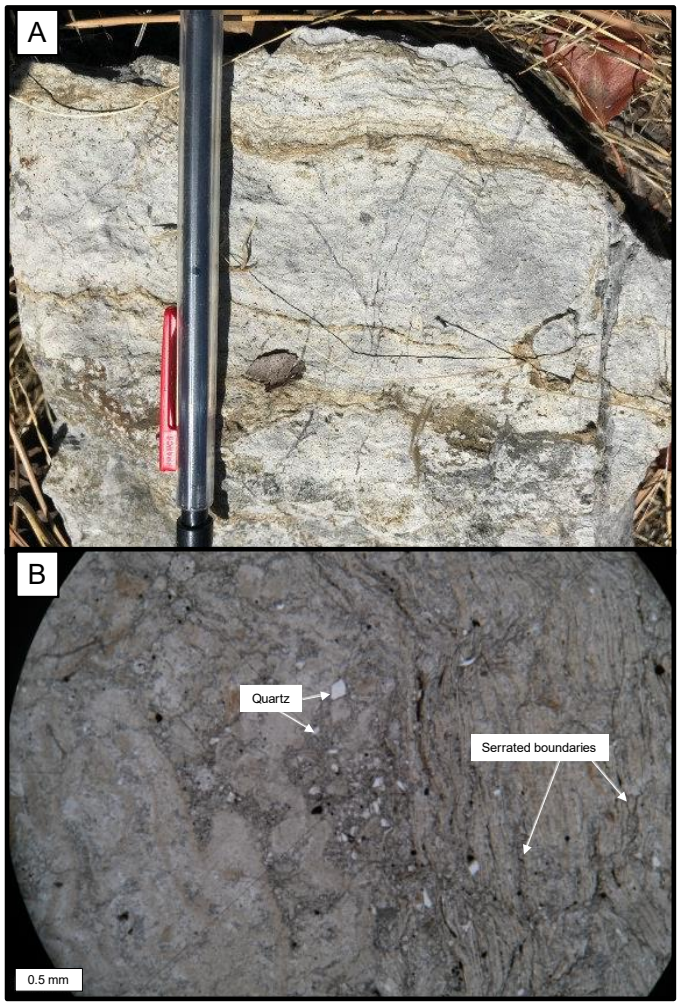

Figure 8: A) Field photo showing crinkled laminae in outcrop D. Red pencil clip measures 3.5 cm for scale. B) Photomicrograph taken in PPL showing clotted fabrics (left) and laminated bladed micrite (right). Other features are labeled.

interpreted to be microbial, and frequently disrupted laminated bladed micrite. The sample also contains trapped grains, primarily angular quartz crystals. Stylolites are common throughout the sample (Figure 8).

5.1.8 Outcrop D: Interpretation

The distinctive crinkled laminae of outcrop D are associated with subaerial exposure and desiccation in a peritidal environment (Flügel, 2010). Quartz grains observed in thin section also support a peritidal interpretation. In addition to the laminae, microtextures including peloidal and clotted fabrics, laminated micrite, and trapped grains point to a microbial (stromatolitic) origin for this sample.

5.1.9 Outcrop E: Description

Outcrop E is separated from outcrop D by ~2 m of colluvium-covered section. There are no clear structural discontinuities present between the two outcrops. Outcrop E is

Figure 9: Field photo of outcrop E. Red pencil clip measures 3.5 cm for scale.

composed of dark grey, thinly bedded (~5 cm) bioturbated wackestone containing small (<0.5 mm) unidentified skeletal debris and visible burrows (Figure 9).

5.1.10 Outcrop E: Interpretation

The high mud content in outcrop E indicates deposition in a low-energy environment, while heavy bioturbation and increased bedding thickness compared to outcrops A and B suggest a shallow water environment able to support abundant burrowing fauna. This outcrop is broadly interpreted to represent a quiet subtidal environment such as a lagoon.

5.1.11 Overall Interpretation: Eagle Creek

Together, the five outcrops interpreted at Eagle Creek point to a shallowing-upward sequence capped off by a return to a deeper water environment. Outcrops A, B, and C represent a shallowing-upward trend. The breccia at the top of outcrop C is indicative of a drop in sea level, and possible sub-aerial exposure. Outcrop D is strongly indicative of a shallow peritidal environment. This outcrop has not (to my knowledge) been described at this location by previous workers, and calls into question previous interpretations of the Eagle Creek locality as an entirely deep-water facies (Nolf, 1966; Follo, 1994; Stanley et al., 2008). While it is possible that the stromatolites were transported via turbidity current from their growth location to a deep water depositional environment, a very large (e.g. house sized) block would have had to be transported in order to preserve such a sizeable outcrop (outcrop D). A debris flow large enough to transport such a block would leave abundant coarse debris nearby, and none was seen at this location or reported by previous workers, making the debris flow hypothesis unlikely. In the absence of evidence of transportation, the in-situ stromatolites observed in outcrop D are interpreted to represent

a peritidal environment that caps an overall shallowing-upward trend. Finally, outcrop E is interpreted as a return to a deeper water environment. The classification and interpretation of each of the samples collected at Eagle Creek are summarized in Table 2, at the end of section 5.3.

5.2 Summit Point

Summit Point is located ~8 km to the northeast of the Eagle Creek locality (Figure 3). Stratigraphically, the rocks at Eagle Creek underlie, overlie, and are laterally equivalent to those at Summit Point (Stanley et al., 2008). Outcrops at this location occur from the fire lookout on top of the peak down to Twin Bridges creek at the base of the mountain, covering ~1.5 km^2. I did not study the stratigraphy at Summit Point in depth, so rather than breaking the locality into outcrops as with Eagle Creek, I have instead divided it into three locations, which represent areas where samples were collected. The inferred relationships between the three locations are summarized in Figure 10. The MBF exposure at Summit Point has also been described by previous workers including Martindale et al. (2012), Follo (1994), Stanley et al. (2008), Stanley and Senowbari-Daryan (1986) and others. Some of their primary observations are included in the descriptions below.

I begin by interpreting the outcrops each sample was collected from, then present an interpretation of the locality by drawing from my own observations and those of previous workers.

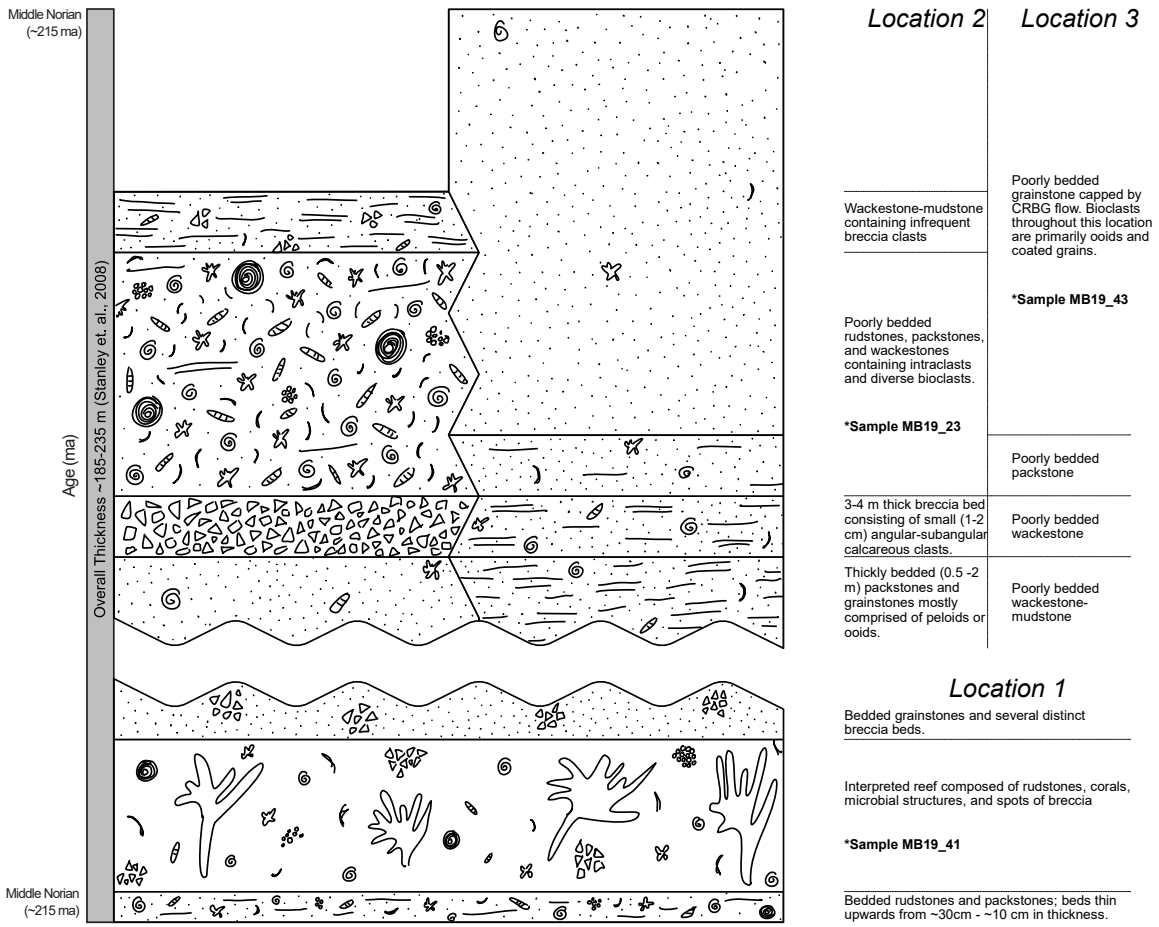

Figure 10: Stratigraphic column for the Summit Point section of the Martin Bridge Formation, Wallowa Mtns, OR. Break between the lowermost and uppermost portions of the column indicates unobserved section. The upper left and upper right sections of the column are interpreted to be laterally equivalent, and there is unobserved section between them. Relative stratigraphic positions are not well constrained, however, and are primarily based on Stanley et al. (2008). See figure 4 for legend.

5.2.1 Sample Location 1: Description

Sample location 1 represents the base of the MBF exposed at Summit Point. The location consists of two outcrops separated by a ~3 m scree slope: (1) a sheer, medium-grey limestone cliff face ~5 m tall that is above (2) ~1.5 m of bedded medium-grey rudstones (Figure 11). The beds in the lowermost outcrop thin upwards, ranging in thickness from ~30 cm at the base of the section to ~10 cm at the top of the section. Secondary calcite veins are common in this outcrop.

The uppermost outcrop is massive and discontinuous along strike. The rocks in this outcrop are grain-supported and range from rudstones and packstones to grainstones. Small patches (~20 cm or less) of breccias and conglomerates consisting of mostly small (<5 cm) clasts appear in spots, and large branching coral heads (1 m or less in diameter) are visible in several places but are not predominant (Figure 11). In addition to branching coral heads, positively identified allochems include sponges, bivalves, and round allochems interpreted as ooids or peloids. Martindale et al. (2012) also described large microbial features in this outcrop.

Sample MB19_41 was collected from a patch of branching coral near the top of the cliff face. In thin section however, MB19_41 shows only one small (~1 cm) piece of coral. The remainder of the sample is composed of mud, skeletal grains, cements, and small amounts of chert (Figure 11).

5.2.2 Sample Location 1: Interpretation

Shells in this outcrop tend to be broken and very little mud is present, indicating a high energy depositional environment. The structure of the outcrop and the depositional texture observed in MB19_41 lead me to interpret this section as a reef. This interpretation is supported by previous workers, who interpret the Summit Point member to represent a reef system on the outer edge of a carbonate platform (Stanley and Senowbari-Daryan, 1986; Martindale et al., 2012).

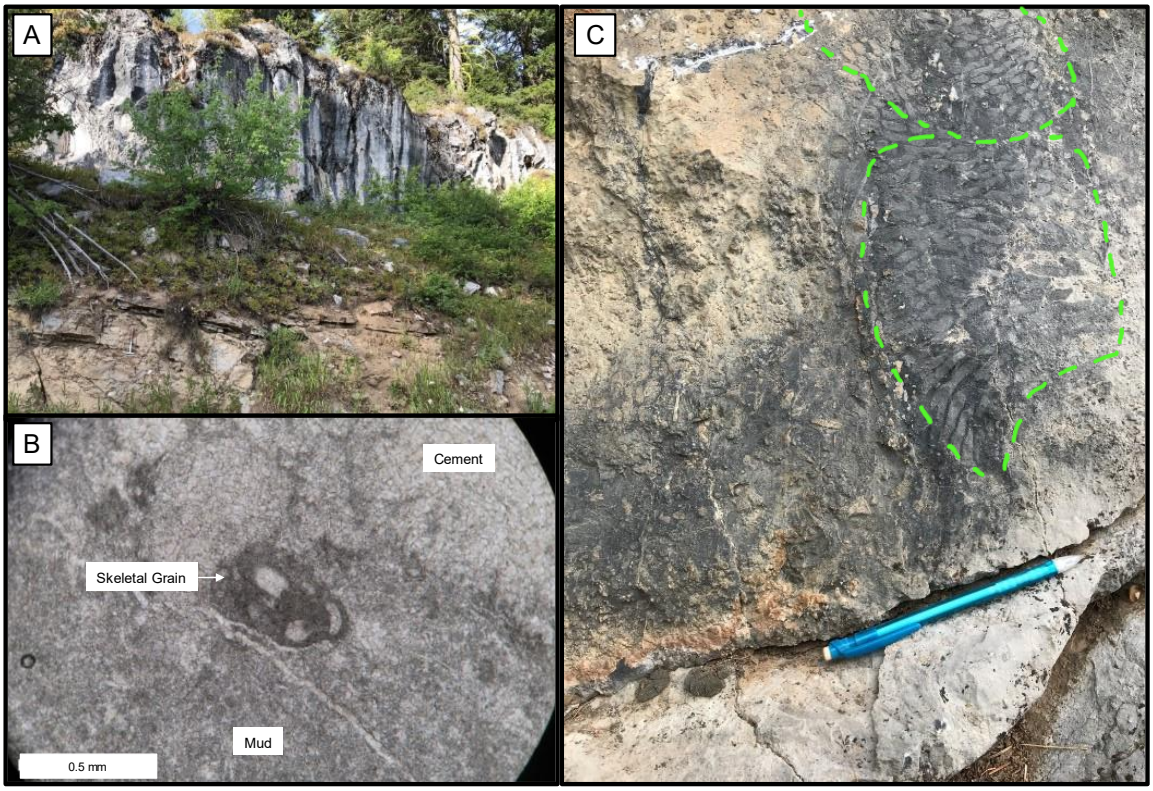

Figure 11: A) Location 1, showing outcrop 1 in background and outcrop 2 in foreground. B) Photomicrograph taken in PPL showing textures observed in sample MB19_41. C) Branching coral head as seen in outcrop at Summit Point. Sample MB19_41 was collected from this outcrop. Pencil is 15 cm long for scale.

5.2.3 Sample Location 2: Description

Sample location 2 is located upsection of sample location 1 based on my own strike /dip measurements and the work of Stanley et al. (2008) (Figure 10). At this location, thickly (0.5 – 2 m) bedded outcrops of light-medium grey limestone strike WSW-ENE along the slope. The lowermost outcrops range from packstone to grainstone and are mostly comprised of small rounded grains (peloids or ooids). A distinctive thick (~3-4 m) breccia bed consisting of small (1 – 2 cm) angular – subangular calcareous clasts is located near the top of these outcrops. Above the breccia bed, outcrops are characterized by abundant and diverse bioclasts in lithologies ranging from wackestone / floatstone to packstone /

rudstone (Figure 12). Intraclasts are common. Positively identified allochems in this location include branching corals, oncolites, bivalves, snails, and crinoids. The uppermost ~5 m of beds that I observed in this location are dark grey in color and distinctly more muddy than the remainder of the section. Sparse allochems and breccia chunks are embedded throughout.

Sample MB19_23 was collected from the middle beds at sample location 2. It is an oncolite rudstone characterized by several large (~4-6 cm) sub-spherical oncoids in a matrix of smaller skeletal grains, intraclasts, and mud (Figure 12).

In thin section, sample MB19_23 is dominated by a large (~5 cm diameter) oncoid. The core of the oncoid is composed of interlocking coarse calcite that fines outward (Figure 12). The layers of the oncoid are composed of mud and contain inclusions of coarse calcite and quartz crystals. The remainder of the sample is made up of skeletal material and coated grains. A stylolite is visible between the oncoid layers and the remainder of the sample (Figure 12).

5.2.4 Sample Location 2: Interpretation

The outcrops at sample location 2 are thickly (meter scale) bedded, lighter in color and characterized by abundant and diverse bioclasts, indicating a generally shallow-water environment (James and Jones, 2016). While oncoids of the type observed in sample MB19_23 are typically associated with moderate to high energy, wave washed environments, the poor sorting of grain sizes in MB19_23 indicates that it was deposited in a low-energy environment where mud and small skeletal grains could also settle (Flügel,

2010). The sample is therefore interpreted as representing the calm margin of a higher-energy open shoal.

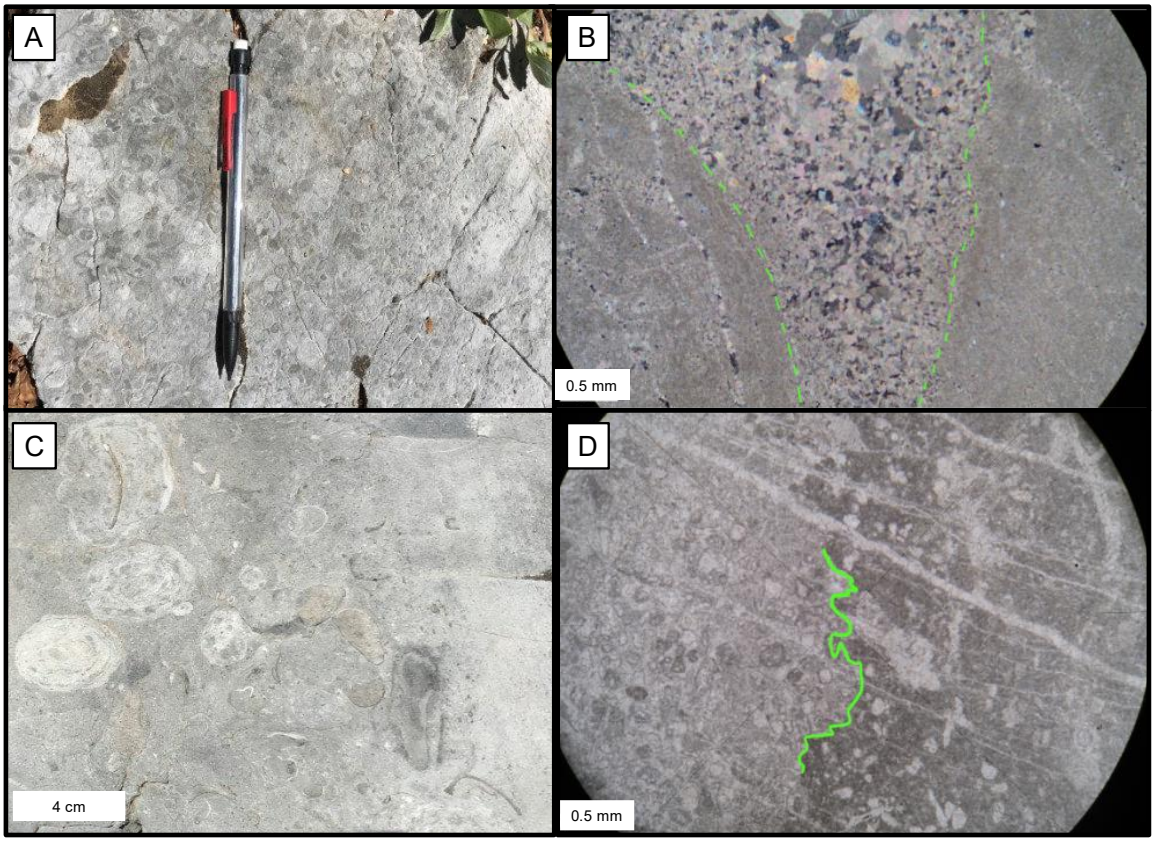

Figure 12: A) Field photo of a rudstone found at sample location 2. Red pencil clip measures 3.5 cm for scale. B) Photomicrograph taken in XPL showing the core of the oncoid (outlined in green) and the surrounding muddy layers. C) Field photo of sample MB19_23. D) Photomicrograph taken in PPL that shows the stylolite (partially outlined in green) which separates the muddy oncoid layers (right) and the surrounding packstone (left).

5.2.5 Sample Location 3: Description

Sample location 3 is located ~300 m ENE along strike (up the modern day slope) from sample location 2. Measured bedding orientations indicate that this location is more or less laterally equivalent to sample location 2. Bedding at this location is difficult to discern because the outcrops are heavily jointed; my best estimates of bedding thickness range from 10 – 50 cm. The outcrops are light grey in color, and the fabric is composed primarily

of ooids and coated grains (Figure 13). Mud content fluctuates from bed to bed, but overall the rocks grade upsection from wackestone to grainstone over a distance of ~20 m. Above the 20 m mark, rocks appear to remain primarily grainstones until the top of the formation, where they are terminated by the CRBG.

Sample MB19_43 was taken ~20 m above the base of the section exposed at sample location 1, in an area composed of mostly ooid grainstones. Thin section analysis reveals that the sample contains two distinct lithologies, separated by a stylolite. The first lithology is a grainstone composed of moderately oriented coated grains, peloids, and ooids. The second is a wackestone that contains these same components, but in a mud-supported matrix. In this second lithology, grains do not appear to be oriented. A small calcite vein is disrupted by the stylolite, suggesting multiple generations of cemetation (Figure 13).

5.2.6 Sample Location 3: Interpretation

The grading of the section from wackestone to well-sorted grainstone suggests that energy levels in the environment increased over time, perhaps indicative of a prograding system, while fluctuations in mud content likely represent small scale changes in sea level. The grains observed in both facies of sample MB19_43 are mostly well sorted ooids and coated grains, which indicate deposition in a shallow subtidal zone. I interpret this sample to represent an open, moderate to high energy shallow water environment on the shelf of a carbonate platform.

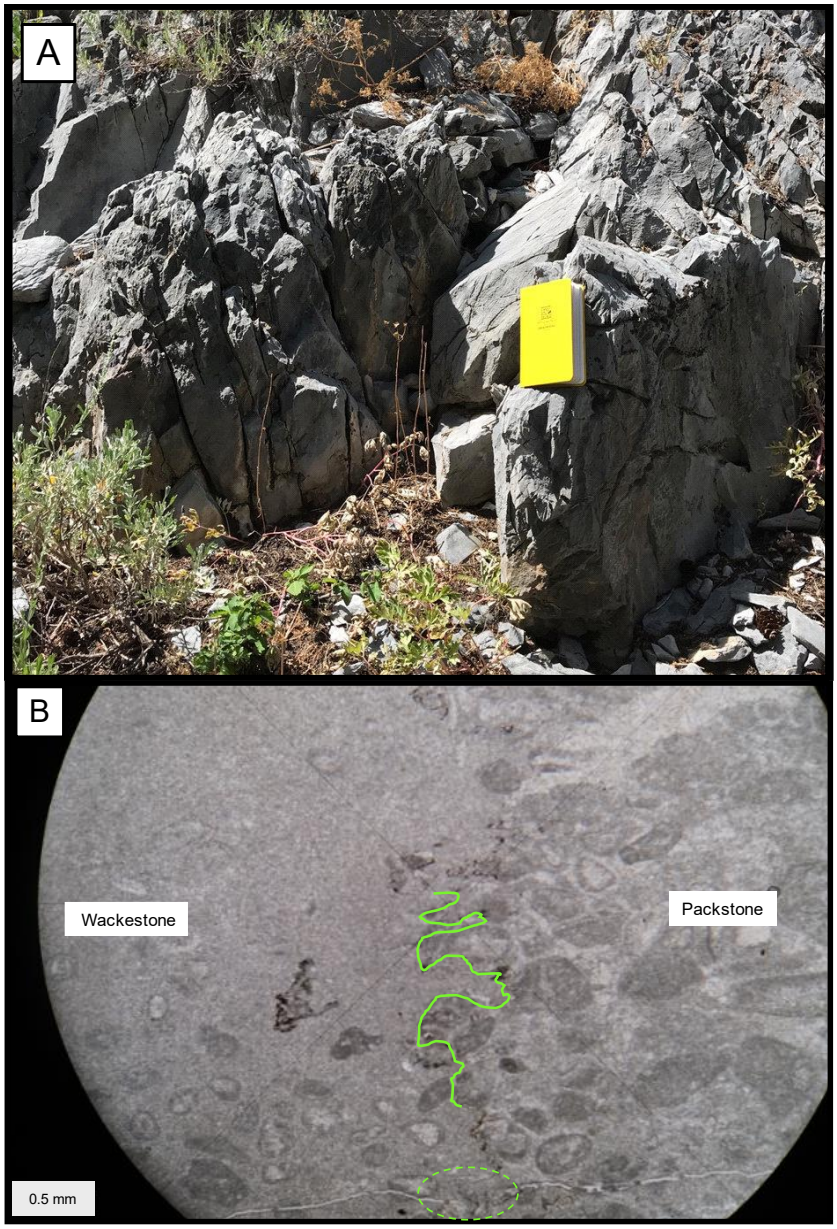

Figure 13: A) Outcrop view of sample location 3. Yellow field notebook measures 19 cm for scale. B) Photomicrograph taken in PPL showing a wackestone (left) and packstone (right) separated by a stylolite, partially outlined in green. A small vein running across the bottom of the image is cut by the stylolite (dashed circle).

5.2.7 Overall Interpretation: Summit Point

Stratigraphic locations described at Summit Point paint a broad picture of a prograding / shallowing upward system. The reef at location 1 is overlain by shallow platform sediments (locations 2 and 3) that show evidence of shallowing upsection. However, the full extent

and relative stratigraphic positions of the outcrops at Summit Point were not covered by this study, providing an opportunity for future research. My interpretations generally align with previous researchers' interpretations that location 1 represents a reef, while locations 2 and 3 are comprised of shallow platform sediments (Stanley and Senowbari-Daryan, 1986; Follo, 1994; Stanley et al., 2008; Martindale et al., 2012). The classification and depositional environment interpretation of samples collected at Summit Point are summarized in Table 2.

Table 2: Classification and interpretation of samples analyzed in this study

Sample	Classification	Interpreted Depositional Environment	Evidence
MB19_01	Mudstone	Distal carbonate slope	Thin, discontinuous laminae; channelization; graded bedding; pyrite
MB19_02	Wackestone	Carbonate slope, more proximal than MB19_01	Same bedding as MB19_01, increased grain content
MB19_38	Stromatolite boundstone	Peritidal	Very fine crinkled laminae; trapped quartz grains; peloidal / clotted fabrics; laminated micrite
MB19_41	Rudstone	Reef	Massive outcrop, discontinuous along strike; broken grains; branching corals
MB19_23	Rudstone	Shallow platform margin	Diverse faunal grains including large oncoids; poor sorting; presence of mud
MB19_43	Wackestone / Grainstone	Shallow platform interior	Well sorted ooids and coated grains

6.0 Discussion

6.1 Visual evidence of diagenesis in samples

While all of the samples are preserved well enough to show evidence of their depositional environment, their age makes it unlikely that they were preserved to the present day in the same form in which they were deposited. Visual evidence shows that the samples have been diagenetically altered to some degree. Chemical evidence, which I discuss in the following sections, reveals details about the conditions of alteration in these samples.

On a meter to kilometer scale, the MBF at both Eagle Creek and Summit Point has been folded and subjected to thrust faulting (Stanley and Senowbari-Daryan, 1986; McRoberts, 1990; Martindale et al., 2012). Igneous intrusions (dikes) have been mapped in the vicinity of both localities (Morriss et al., 2020) (Figure 3). Modeling suggests that alteration stemming from the emplacement of these dikes can extend up to ~100 m from the dike contact (Karlstrom et al., 2019, Murray and Winkelstern, unpublished data). Finally, extrusive material (CRBG) unconformably overlies the MBF exposed at Summit Point.

At a hand sample scale, evidence of alteration is present in most samples. Diagenetic minerals observed in the samples include calcite veins and mineralization on surfaces, iron sulfides, and quartz (silicification). Diagenetic textures are also abundant. These include stylolite, indicating pressure dissolution within the rock, and micritized rims on grains, an early diagenetic process that occurs as microbes / algae nibble away at the edges of grains.

Comparison to Whalen's (1985) diagenetic history at Hells Canyon indicates that all of the diagenetic features observed in my samples are also present at Hells Canyon, which Whalen interprets as representing early diagenetic processes that occurred before

geochemical ‘peak’ alteration. Of particular note is that Whalen recorded multiple generations of dolomitization in his diagenetic history, while dolomitization features are absent in the samples I collected. This may simply be explained by the geographic and geologic differences between the two locations; the BC Creek facies exposed at Hells Canyon is thought to represent a more shallow and evaporitic environment than the Eagle Creek and Summit Point facies described in this study (Whalen, 1985; Stanley et al., 2008).

6.2 Discussion of Geochemical Results

In this section I address two questions: (1) at what time did peak diagenetic alteration occur, and (2) what are the most likely controls on diagenetic alteration? The following addresses both these questions, working from the largest scale to the smallest. The previous sections, which assign texture and depositional environment to the samples, will be referenced in discussing possible controls on alteration.

6.2.1 Timing of Alteration

Synsedimentary Marine

The isotopic composition of original formation water influences the ultimate isotopic composition of marine carbonates. At the time of primary carbonate deposition, ocean water fills the pore space. If the rock is diagenetically altered in an open system at or near the time of deposition, diagenetic carbonates are likely to form from ocean water with a similar isotopic composition. As time goes on, the nature of the hydrologic system and the composition of the alteration water is likely to change. Waters from non-oceanic sources (meteoric, magmatic, metamorphic) and water-rock interactions may shift the isotopic composition of formation waters over time (Figure 14).

In this study, back-calculated formation waters are more positive than would be expected for an oceanic source. Assuming open system behavior, formation water $\delta^{18}O$ values are relatively positive in both the Eagle Creek (average value = 9.63‰, range of values = 7.69‰ – 12.74‰) and Summit Point (average value = 10.58‰, range of values = 6.55‰ – 15.00‰) localities, compared to the isotopic composition of Triassic seawater: ~1.5‰ $\delta^{18}O$ (James and Jones, 2016).

The $\delta^{13}C$ values in this dataset are only slightly lower than (average value 1.14‰) expected for Triassic ocean water, which was ~2.0‰ $\delta^{13}C$ (James and Jones, 2016). The lack of a significant change in $\delta^{13}C$ values is not surprising; fluids contain significantly less carbon than oxygen and as such $\delta^{13}C$ values are thought to be less affected by diagenesis (Hoefs,

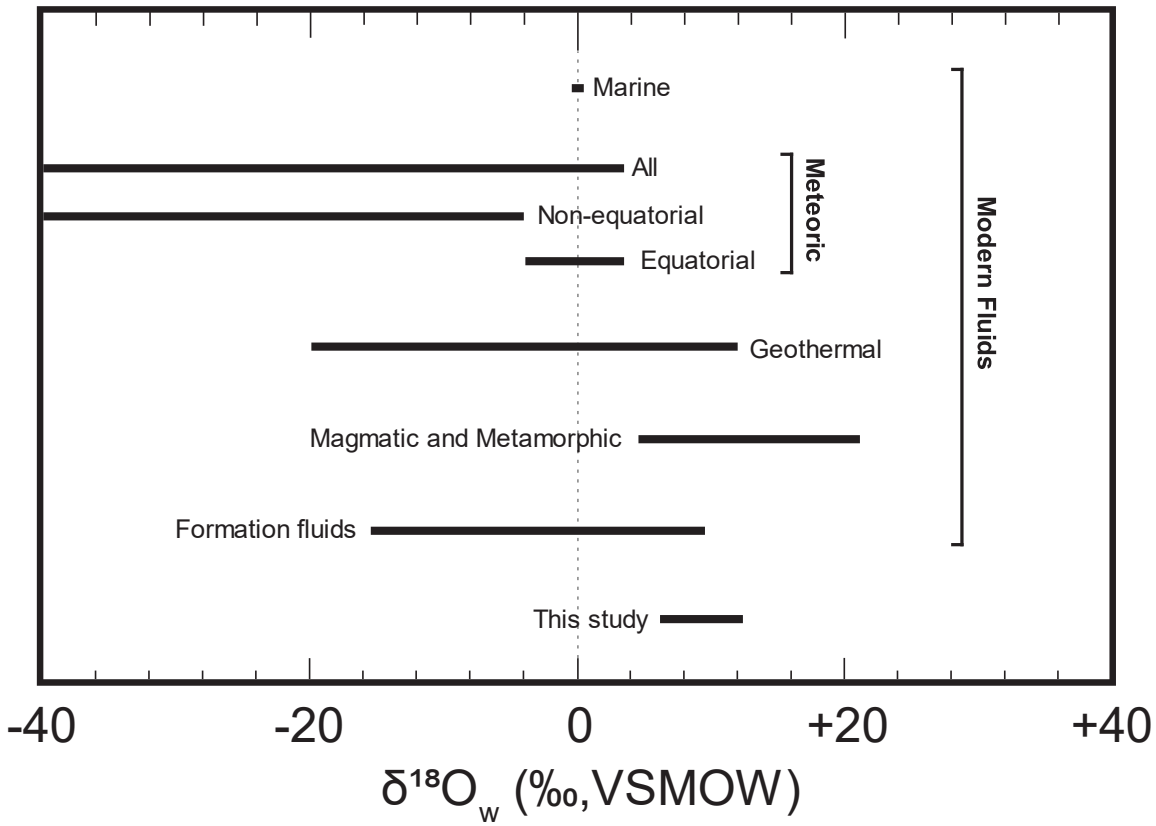

Figure 14: Oxygen isotope ranges of modern and reconstructed Mesozoic fluids, as well as the range of $\delta^{18}O_w$ values found in this study. Figure adapted from Loyd et al. (2015)

2018). The strongly positive $\delta^{18}O_w$ values, as well as high temperatures (based on Δ_{47} data, see Table 1) at the time of carbonate mineralization, indicate that these carbonates no longer retain their original, oceanic, isotopic signature.

Early Meteoric Diagenesis

Early diagenesis occurs during burial up to a few hundred meters depth, where temperatures are typically <140° C (James and Jones, 2016). This environment is referred to as the meteoric diagenetic environment. Diagenetic changes that occur in this phase are thought to be marked by a positive correlation between the $\delta^{18}O$ and $\delta^{13}C$ values of carbonate rocks (Allan and Matthews, 1982; Swart and Oehlert, 2018). The correlation arises when meteoric groundwater mixes with marine pore fluids. As the proportion of meteoric water increases, $\delta^{18}O$ and $\delta^{13}C$ both decrease, causing a positive covariant trend. Because the proportional increase in meteoric water is tied to shallowing of the carbonate platform, limestones that have been altered in an early meteoric diagenetic environment show $\delta^{13}C$ and $\delta^{18}O$ decreasing with increasing height in the stratigraphic succession until an exposure surface is reached (Allan and Matthews, 1982).

While my data show a positive covariant trend, I believe it unlikely that early meteoric diagenesis is responsible. If the covariance in my data was tied to early meteoric diagenesis, I would expect to see samples that come from shallow marine or marginal marine environments to cluster where $\delta^{18}O$ and $\delta^{13}C$ values are relatively low, which is not the case (Figure 15). The temperatures recorded at the time of mineralization (based on Δ_{47} data, see Table 1) are also well above what would be expected in a meteoric diagenetic environment (average temperature of my samples is 170.5° C, while the majority of early

meteoric diagenesis is considered occur at temperatures between 20° C and 30° C) (Swart, 2015). Finally, compaction features seen in the majority of my samples suggest that alteration took place during a period of greater overburden than what would be expected in the early meteoric diagenetic environment (see: samples MB19_23, MB19_38, MB19_43) (James and Jones, 2016). For these reasons, these samples are unlikely to retain a strong isotopic signal that can be directly tied to alteration in an early meteoric diagenetic environment.

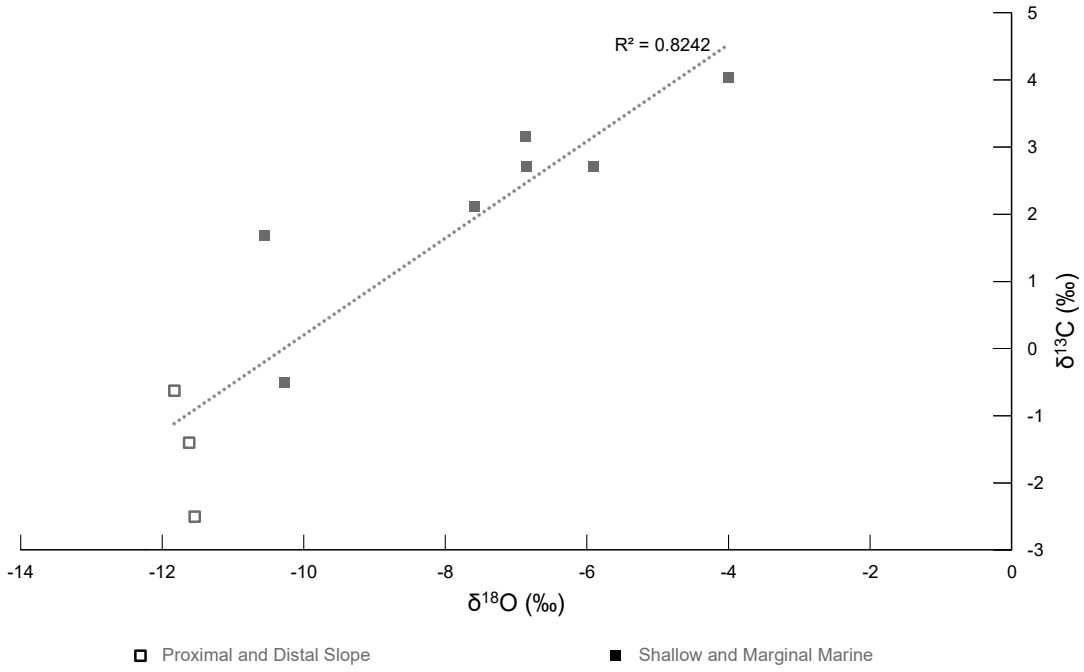

Figure 15: $\delta^{18}O$ vs. $\delta^{13}C$ scatterplot. Samples representing a deeper water environment cluster at the base of the trendline, suggesting that covariance in the data is not tied to early meteoric diagenesis.

Burial Diagenesis

The burial diagenetic environment occurs at depths of several hundreds to thousands of meters. Pore waters in this environment have typically been modified from their original isotopic composition by isotopic exchange with the surrounding rock and interaction with

secondary fluids under elevated temperature and pressure conditions (James and Jones, 2016). Compaction features and high mineralization temperatures observed in my samples are indicative of a burial diagenetic environment.

The range of temperatures associated with my samples presents an opportunity to further refine the depth and timing of alteration. Approximately 2 km of sedimentary rock directly overlies the MBF, implying a burial-associated temperature of only ~50° C (assuming a geothermal gradient of 25 °C/km) (Follo, 1994; Arndt, 2011). An unconformity between the uppermost member of the sedimentary overburden (Coon Hollow formation, see Fig. 1.2 in Follo, 1994) and the modern CRBG flows, which currently cap the section, represents ~140 ma of missing time. It is certainly possible that a thicker sedimentary overburden was present at some point and has since been eroded away. However, the highest temperature associated with my samples (245 °C, sample MB19_38) would require nearly 10 km of overburden, or 8 km of missing section. Given the largely quiescent history of the Wallowa terrane between accretion (~150 ma) and uplift (~15 ma), it is highly unlikely that such a large sedimentary overburden would have accumulated and then eroded away (Hales et al., 2005; LaMaskin et al., 2015).

Magmatic Heat Source / Timing of Alteration

To explain the high temperatures recorded by my samples, a heat source outside of burial heating was likely present. There are three possible candidates: frictional heating from fault slip, CRBG dikes (emplaced mid-Miocene) and the Wallowa batholith (emplaced early Cretaceous) (Figure 1, Figure 3). Frictional heating from fault slip has not been shown to affect Δ_{47} values outside of the fault mirror region (~1 μm area in which slip and shear

heating are focused) (Siman-Tov et al., 2016). CRBG dikes are relatively small in size and were emplaced and cooled over a much shorter period of time than the Wallowa batholith. Outcrops of the Wallowa batholith are over a kilometer from my sample locations. However, the size and longevity of this heat source make it the preferred candidate to explain the relatively high temperatures of carbonate alteration observed in my samples.

The necessity of an outside heat source to drive the elevated temperatures recorded in my samples allows me to tie the timing of alteration to the emplacement of the Wallowa batholith. Geochemical evidence indicates that the batholith was emplaced in early Cretaceous time (140.2 – 125.6 ma) (Johnson et al., 2011). Therefore, I would place the timing of alteration in my samples as most likely occurring during early Cretaceous time, during the period of maximum heat flux in the region.

6.2.2 Alteration Controls

The following sections utilize data analysis and modeling to understand the conditions of post-depositional alteration observed in these samples. Five proxies are used for alteration: $\delta^{18}O_{carb}$, $\delta^{18}O_{water}$, $\delta^{13}C$, temperature (Δ_{47}), and W/R ratio. Here, I interpret controls on diagenetic alteration, beginning at the largest scale and working to the smallest.

Open vs. Closed System Alteration

Hydrologic systems exist on a continuum between purely open (e.g. fluid is refreshed continually from an outside source) and purely closed (e.g. fluid is sealed within the rock and is not refreshed at all). In a purely open system, the $\delta^{18}O_w$ values calculated from $\delta^{18}O$ values represent the initial fluid $\delta^{18}O$. For samples located in the same geographic area, this value should be the same for all samples over time, and align with a primary source

fluid (meteoric precipitation, ocean water, etc). In a purely closed system, $\delta^{18}O_w$ represents an evolved version of the initial primary source fluid $\delta^{18}O$. In closed systems, $\delta^{18}O_w$ is dependent on 1) temperature 2) water-rock (hereafter referred to as W/R) ratios and 3) the initial isotopic compositions of the fluid and the rock (Clark, 2015). Samples that have undergone closed-system re-equilibration should yield $\delta^{18}O_w$ values that positively correlate to carbonate precipitation temperatures (Δ_{47}), indicating that the fluid was evolving during carbonate precipitation. While there are certainly structural complications to this trend, one can generally assume that systems become more closed with increasing burial depth (Hoefs, 2018). My data exhibit a positive correlation between $\delta^{18}O_w$ and temperature at both the Eagle Creek and Summit Point localities (Figure 16), indicating that diagenetic alteration in these locations is best modeled assuming the hydrologic system was closed.

Fluid Provenance / Environment of Re-Equilibration

The reconstructed temperature and $\delta^{18}O_w$ ranges for my samples overlap with known values for a variety of subsurface environments. This range of $\delta^{18}O_w$ values is consistent with three possible initial sources: 1) magmatic and metamorphic fluids, which are commonly 6 to 25‰, 2) seawater, which is tightly constrained at ~ 0‰, or 3) meteoric water, which ranges broadly from -40 to 4‰ (Figure 14). Due to the closed nature of the system in which alteration occurred, water-rock interactions likely caused the $\delta^{18}O$ value of the fluid to evolve from that of its initial source to a different (typically higher) $\delta^{18}O$ value. (Loyd et al., 2015; Hoefs, 2018).

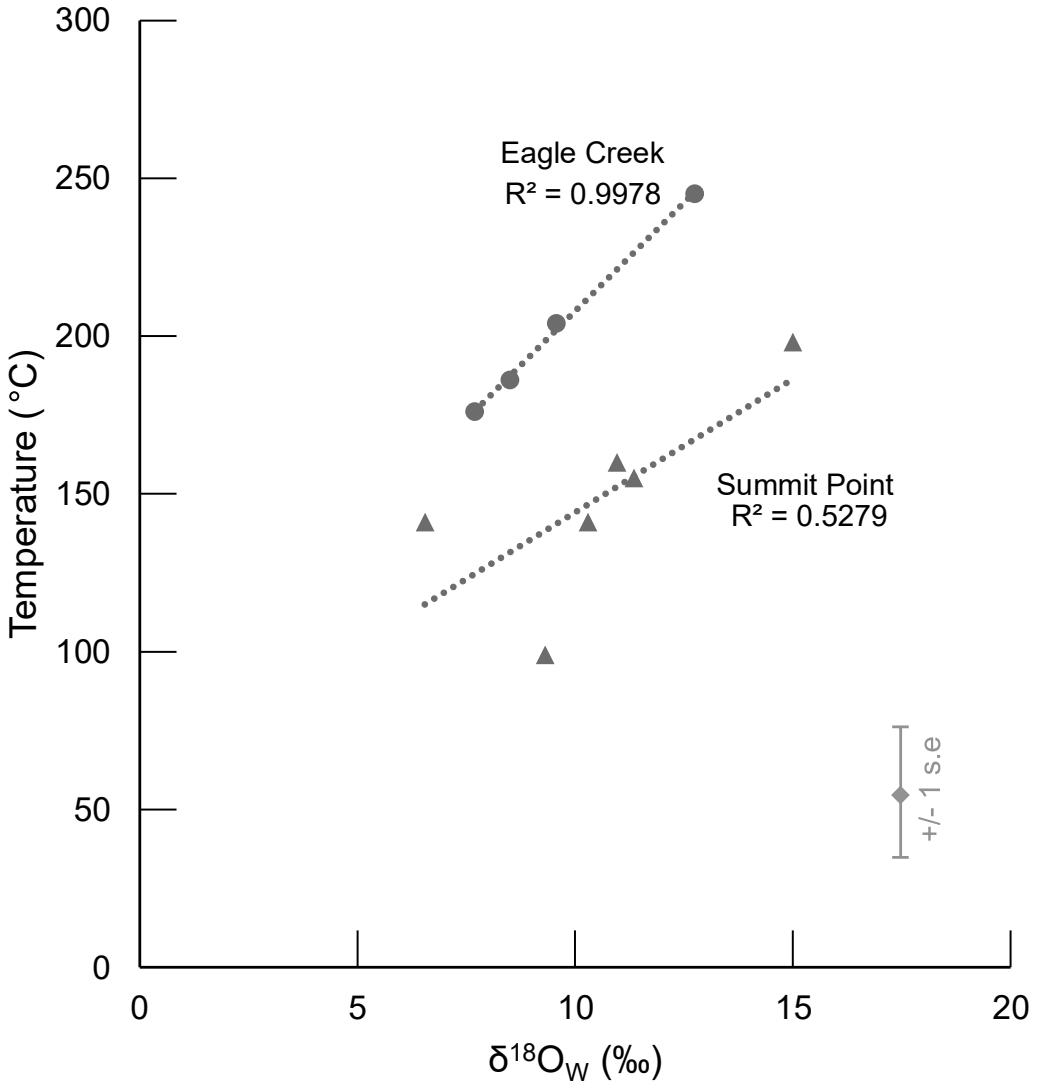

Figure 16: Graph showing $\delta^{18}O_w$ vs. temperature plotted by location. Temperature positively covaries with $\delta^{18}O_w$, indicating that the hydrologic system at the time of alteration was primarily closed. The difference in temperature between the two locations is likely not significant, considering large analytical error.

Initial fluid $\delta^{18}O_w$ values representing the three sources listed above are used in Figure 17, which models the alteration trajectories of a marine carbonate in a closed system at different initial fluid $\delta^{18}O_w$ values. Temperature and $\delta^{18}O_w$ values from the samples analyzed in this study are plotted over the modeled trajectory lines, showing alignment with trajectories generated from initial fluid values between 0 and -10‰. Fluid trajectories modeled for an initial fluid value of +10‰ (representative of magmatic / metamorphic

waters, see Figure 14) do not overlap with my data points (Figure 17). This indicates that despite the proximity of the Wallowa batholith at the time of diagenesis, magmatic and metamorphically derived fluids are unlikely to have been a significant component in the initial fluid.

My $\delta^{18}O_w$ values best overlap with models requiring an isotopically depleted initial fluid, consistent with meteoric water (Figure 14, Figure 17). Meteoric water (in the form of groundwater) is the most abundant form of water found in continental rocks and, unlike a magmatic / metamorphic fluid, would not require significant transport in the subsurface (Clark, 2015).

Meteoric water could have infiltrated the MBF at any point between early meteoric diagenesis, shortly following deposition, to the early Cretaceous period when high temperatures derived from the Wallowa batholith 'set' the isotopes at their current values.

The $\delta^{18}O$ value of precipitation varies with latitude and elevation. To test my hypothesis that alteration took place in the early Cretaceous period using formation fluid derived from meteoric water, I calculated the $\delta^{18}O$ value of precipitation at the approximate latitude and elevation of the Wallowa terrane in both the late Triassic and early Cretaceous (see Appendix). In the late Triassic, assuming a paleolatitude of ~24° and sea level elevation, the $\delta^{18}O$ value of precipitation would have been approximately -3.8‰ (Harbert et al., 1995). In the early Cretaceous, assuming a paleolatitude of ~41° and sea level elevation, precipitation would have had a $\delta^{18}O$ value of approximately -6.5‰ (Wyld and Wright, 2001; Bowen and Wilkinson, 2002). Both of these starting fluid values in the closed-system evolution model yield trajectories that fit my data well at a W/R ratio of ~0.3 (Figure 18).

A scenario in which meteoric water infiltrates into rock and subsequently becomes heated has also been reported by Loyd et al. (2015), who found evidence of diagenetic alteration in Neoproterozoic carbonates by an initial fluid with oxygen isotope values between -10 and -15‰, at temperatures up to 370 °C.

In summary, my data best fit a model in which an isotopically depleted (meteoric) initial fluid evolved in a primarily closed system at a W/R ratio between 0.1 and 0.5 (Figure 18). The necessity of a heating source beyond the geothermal gradient to account for high temperatures at the time of alteration allows me to correlate the timing of peak carbonate alteration to the emplacement of the Wallowa batholith in early Cretaceous time.

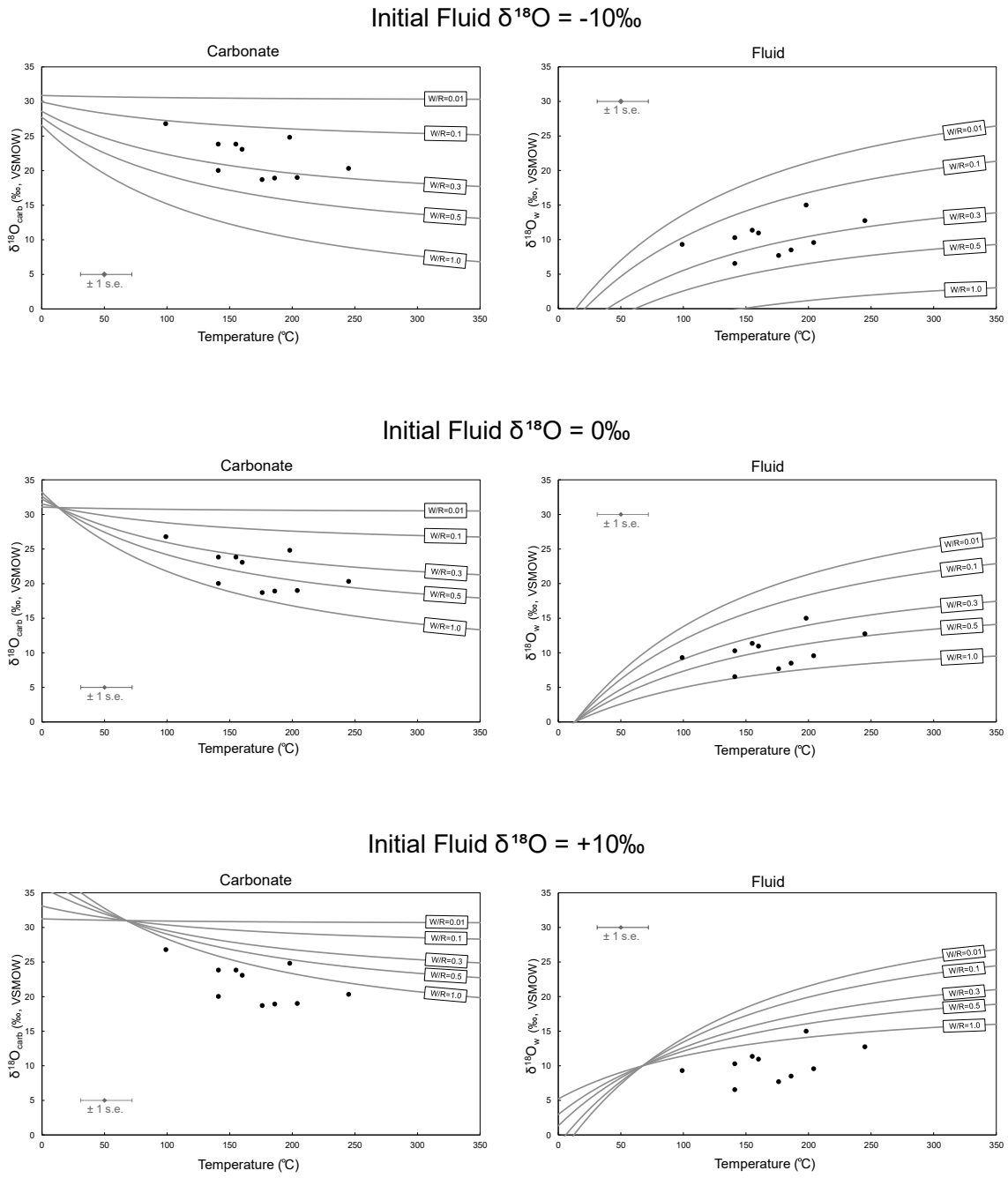

Figure 17: Cross plots of clumped isotope temperature (Δ_{47}) and oxygen isotope data ($\delta^{18}O_{carb}$ and $\delta^{18}O_w$) from the study locality. Left plots show temperature and $\delta^{18}O_{carb}$ relationships and right plots show temperature and $\delta^{18}O_w$ relationships. The plots also show evolutionary trajectories for different water-rock ratios (W/R) as they pertain to initial fluid and carbonate mineral (labeled for each set of plots) isotopic compositions. The details of the W/R model are provided in section 3.4.2. Average long-term standard reproducibility in temperature estimates provided as +/- 1 standard error.

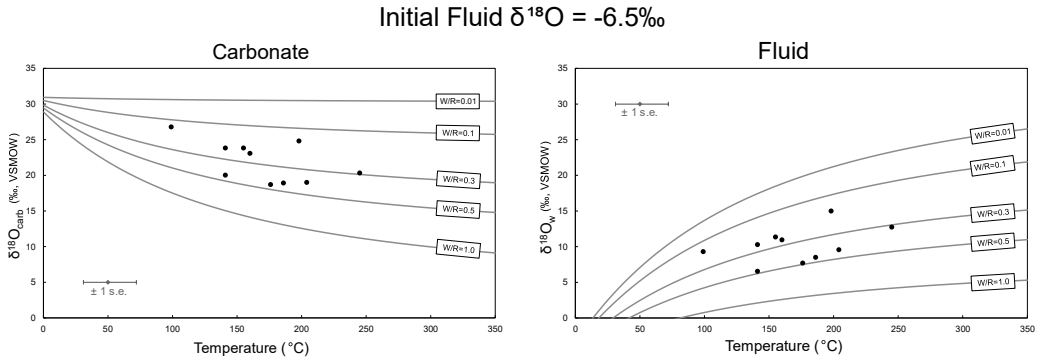

Figure 18: Cross plot of clumped isotope temperature (Δ_{47}) and oxygen isotope data ($\delta^{18}O_{carb}$ and $\delta^{18}O_w$) from the study locality, plotted over evolutionary trajectories for different water-rock ratios (W/R) as they pertain to an initial fluid isotopic value of -6.5‰. Using an initial fluid isotopic value of -3.8‰ yields very similar results (not shown). The details of the W/R model are provided in section 3.4.2. Average long-term standard reproducibility in temperature estimates provided as +/- 1 standard error.

Water / Rock Ratio

This final section considers some possibilities for controls on inter- and intra-sample variation in the geochemical alteration proxies. Modeling that shows the geochemical evolution of a closed system with a starting fluid $\delta^{18}O$ value of -6.5‰ (Figure 18) suggests that there are differences in W/R ratios between samples, as well as, in some cases, individual spots on the same sample. W/R ratios negatively covary with both $\delta^{18}O$ and $\delta^{13}C$ values, indicating that W/R ratio is tied to the ultimate geochemical composition of the samples. W/R ratio is also a proxy for alteration in its own right: in a closed hydrologic system, the ratio of water to rock affects the degree of geochemical evolution experienced by both the water and the rock (Figure 17). In systems where the W/R ratio is high ("water-buffered"), the rock will experience a greater geochemical change than the water, relative to their respective starting compositions. In systems where the W/R ratio is low ("rock-buffered"), the water will experience the greater geochemical change of the two (Clark, 2015).

Modeling done in Figure 18 using -6.5‰ water as a starting fluid shows that different samples likely evolved under differing W/R ratios. The data can be grouped by W/R ratio (Table 3).

Table 3: W/R ratio compared to locality and spot description

Approximate W/R Ratio	Sample	Locality	Spot Description
< 0.3	MB19_43	SP	Spot drilled in a grainstone characterized by moderately oriented coated grains, peloids, and ooids
< 0.3	MB19_41_LOC2	SP	Spot drilled in the matrix surrounding a large branching coral. Matrix material is comprised of mud, skeletal grains, cements, and small amounts of chert
< 0.3	MB19_41_LOC1	SP	Spot drilled in a coral branch
< 0.3	MB19_23_LOC3	SP	Spot drilled in the matrix of a rudstone containing a large oncoid (MB19_23_LOC1 and LOC2). Matrix is primarily comprised of skeletal material, coated grains, and small intraclasts.
< 0.3	MB19_23_LOC2	SP	Spot drilled in the core of an oncoid. Oncoid core is composed of interlocking coarse calcite that fines outward.
0.3	MB19_38	EC	Spot drilled in a stromatolite boundstone characterized by very fine crinkled laminae; trapped quartz grains; peloidal / clotted fabrics; laminated micrite
> 0.3	MB19_23LOC1	SP	Spot drilled in the layers (word choice?) of an oncoid. Oncoid layers are composed of mud and contain inclusions of coarse calcite and quartz crystals.
> 0.3	MB19_02	EC	Spot drilled in a brachiopod shell imprint in a wackestone with the same bedding features as MB19_01
> 0.3	MB19_01_LOC2	EC	Spot drilled in the light-colored band of a mudstone characterized by thin, discontinuous laminae, channelization, graded bedding, and pyrite
> 0.3	MB19_01_LOC1	EC	Spot drilled in the dark-colored band of a mudstone characterized by thin, discontinuous laminae, channelization, graded bedding, and pyrite

Modern Geography

One trend shown by W/R ratio grouping (Table 3) is that the Eagle Creek samples all have a higher W/R ratio (~0.3 – 0.5), while the Summit Point samples tend towards lower W/R ratios, ranging from ~0.1 – 0.3. This could indicate that the Summit Point locality was buried more deeply than the Eagle Creek locality at the time of alteration (assuming W/R decreases with increasing depth). It could also indicate that water infiltration was stronger at Eagle Creek than Summit Point, perhaps due to the permeability of the surrounding rocks or the structural complexities of the area (McRoberts, 1990; Follo, 1994).

Texture (Porosity, Permeability)

The rocks at Eagle Creek are all mud-supported, while the rocks at Summit Point are mostly grain-supported. Rocks with mud-dominated textures tend to retain water at depth due to low permeability, which might explain why the rocks at Eagle Creek retained more water during the period of alteration than their counterparts at Summit Point (Bayer and Wetzel, 1989; Neuzil, 1994; Broichhausen et al., 2005; Yang and Aplin, 2010). Interestingly, MB19_23_LOC1 comes from a sample collected at Summit Point, but plots with the high W/R samples at Eagle Creek. Two other spots on this sample that I analyzed, representing the oncoid core and the matrix surrounding the oncoid, produced W/R ratios similar to other Summit Point samples (Table 3). This supports my hypothesis that less permeable mud-prone samples are more likely to retain water, leading to higher W/R ratios. In the case of sample MB19_23_LOC1, muddy oncoid layers may have formed a localized zone of low permeability leading to heterogeneous W/R ratios across the individual hand sample.

Localized differences in texture may also explain the discrepancy in W/R ratio between MB19_41_LOC1 (W/R ratio ~0.3) and MB19_41_LOC2 (W/R ratio ~0.1). MB19_41_LOC1 represents a branching coral and MB19_41_LOC2 represents the matrix surrounding it. The matrix in MB19_41_LOC2 is characterized by large amounts of cement, suggesting that there was significant porosity at the time of alteration. Relatively high porosity in sample MB19_41_LOC2 may indicate high permeability as compared to the solid coral branch represented by spot MB19_41_LOC1.

Depositional Environment

The rocks at Eagle Creek and Summit Point represent depositional environments ranging from muddy slope to shallow, allochem-rich platform. As discussed previously, the amount of mud present in a given environment does appear to influence diagenesis. While depositional environment can broadly be correlated with mud content, it is not strictly predictive of it. This study has found that depositional environment is not significantly correlated to texture, nor to any of the geochemical proxies used in this study, indicating that depositional environment alone is not a strong control on burial diagenetic alteration in the MBF.

If peak alteration had occurred earlier in the depositional history of the rocks (e.g. in a synsedimentary marine or early meteoric diagenetic environment), depositional environment might have exerted more control on the ultimate geochemical composition of the rocks. For example, in a pre-burial diagenetic environment, a more open hydrologic system would increase the relative importance of alteration fluid chemistry, which in turn is controlled by depositional environment (e.g. shallower = greater meteoric water input,

deeper = less meteoric water input) (Swart and Oehlert, 2018). This and other differences between depositional environments that could impact alteration were overwhelmed by burial, which allowed other controls on alteration to be expressed more strongly.

7.0 Conclusions

The diagenetic history of the Martin Bridge Formation (MBF) is a window into the larger story of the Wallowa terrane. These carbonates formed when the Wallowa terrane was a volcanic island arc bathed in warm, low-latitude waters, and that part of their history is preserved in the rocks' morphology and stratigraphy. The geochemistry of the rocks elucidates the second part of their story: what happened over the 210 million years since deposition.

The purpose of this study was to understand the timing of, and controls on, alteration in the MBF. I hypothesized that two factors would prove to be strong controls on alteration: rock texture, and depositional environment. Based on my data, I found that the three factors which exert the most control over alteration in my samples are: (1) the closed nature of the hydrologic system at the time of alteration (2) the meteoric provenance of the alteration fluid, and (3) the W/R ratio (~0.3) at which alteration occurred.

In analyzing my data, I found that depositional environment did not have a strong effect on alteration, most likely because in these samples, alteration occurred in a burial diagenetic environment where the differences between depositional environment types were muted. If peak alteration had occurred earlier in the depositional history of the rocks, depositional environment might exerted more control on the ultimate geochemical composition of the rocks.

Rock texture does appear to have an effect on alteration in the MBF insofar as it influences permeability, and therefore W/R ratio. This relationship is rather tenuous however – it is based on limited data (n=10), and the differences between those data points are modest. Fully understanding the effect of rock texture on alteration would require a more robust data set, and better understanding of other controls on alteration. If rock texture does exert a significant control on carbonate diagenesis as this study suggests, the absence of mud in a sample may be indicative of lower diagenetic susceptibility when compared to a similar sample containing a high amount of mud.

In the part of the MBF covered by the study area, my results suggest that alteration took place in a closed system, at relatively high temperatures. The burial history of the MBF is not sufficient to account for the temperatures recorded, indicating that alteration must be tied to an outside heat source. The Wallowa batholith is the preferred candidate for the source of this heat; its unique size and longevity are strong indicators that it could have raised the surrounding country rock to the temperatures recorded by my samples. Alteration in my samples is therefore most likely to have occurred during the period in which the Wallowa batholith was emplaced. The batholith has been U-Pb dated to early Cretaceous time (140.2 – 125.6 ma) by Johnson et al. (2011), indicating that samples from my study area were also altered during this time period.

Finally, plotting my data over the closed-system evolution trajectories developed by Banner and Hanson (1990) indicates that the alteration fluid had an initial $\delta^{18}O$ value of 0‰ or less (Figure 17). The early Cretaceous timing of alteration allows me to further

constrain the alteration fluid in my samples as Mesozoic meteoric water with an initial $\delta^{18}O$ value between -3.8 and -6.5‰ (Figure 18).

In summary, the hypothesis that depositional environment affects the expression of diagenesis in the MBF is not supported by this study. This study does indicate that carbonate texture (e.g. amount of mud) affects diagenesis in that it may alter the W/R ratio, resulting in varied isotopic compositions, even down to the hand-sample scale. This interpretation is based on a limited number of data points (n=10), so further research is necessary to confirm or refute this hypothesis.

My data show that the portions of the MBF included in this study were altered in a primarily closed system, at W/R ratios ranging from 0.1 to 0.5 (average value ~0.3), by an initial fluid consistent with Mesozoic meteoric water ($\delta^{18}O$ = -3.8 to -6.5‰). The necessity of a heating source in excess of the geothermal gradient to account for high temperatures at the time of alteration allows me to correlate the timing of carbonate alteration to the emplacement of the Wallowa batholith in early Cretaceous time.

8.0 Opportunities for Future Research

My results suggest that mud-prone carbonates might be more susceptible to diagenesis due to their ability to hold water more effectively than carbonates lacking significant mud. However, the sample size (n=10) and data quality are not sufficient to confirm this hypothesis with certainty. Further research should focus on quantifying the amount of mud in a given sample, and testing how stable isotopes change in a dataset where all other controls (temperature, alteration fluid, hydrologic system) remain relatively constant. In addition, depositional environment as a control on alteration could be more effectively studied in younger rocks, where burial diagenesis has not yet occurred and the primary forms of diagenesis expressed are synsedimentary marine / early meteoric diagenetic.

References

Allan, J.R., and Matthews, R.K., 1982, Isotope signatures associated with early meteoric diagenesis: Sedimentology, v. 29, p. 797–817.

Arndt, N., 2011, Geothermal Gradient, *in* Gargaud, M., Amils, R., Quintanilla, J.C., Cleaves, H.J. (Jim), Irvine, W.M., Pinti, D.L., and Viso, M. eds., Encyclopedia of Astrobiology, Berlin, Heidelberg, Springer Berlin Heidelberg, p. 662–662, doi:10.1007/978-3-642-11274-4_643.

Banner, J.L., and Hanson, G.N., 1990, Calculation of simultaneous isotopic and trace element variations during water-rock interaction with applications to carbonate diagenesis: Geochimica et Cosmochimica Acta, v. 54, p. 3123–3137, doi:10.1016/0016-7037(90)90128-8.

Bayer, U., and Wetzel, A., 1989, Compactional behavior of fine-grained sediments — examples from Deep Sea Drilling Project cores: Geologische Rundschau, v. 78, doi:10.1007/BF01829324.

Bowen, G.J., and Wilkinson, B., 2002, Spatial distribution of □18O in meteoric precipitation: , p. 4.

Brand, W.A., Assonov, S.S., and Coplen, T.B., 2010, Correction for the 17O interference in δ(13C) measurements when analyzing CO2 with stable isotope mass spectrometry (IUPAC Technical Report): Pure and Applied Chemistry, v. 82, p. 1719–1733, doi:10.1351/PAC-REP-09-01-05.

Broichhausen, H., Littke, R., and Hantschel, T., 2005, Mudstone compaction and its influence on overpressure generation, elucidated by a 3D case study in the North Sea: International Journal of Earth Sciences, v. 94, p. 956–978, doi:10.1007/s00531-005-0014-1.

Clark, I., 2015, Groundwater Geochemistry and Isotopes: CRC Press, 438 p.

Daëron, M., Blamart, D., Peral, M., and Affek, H.P., 2016, Absolute isotopic abundance ratios and the accuracy of Δ47 measurements: Chemical Geology, v. 442, p. 83–96, doi:10.1016/j.chemgeo.2016.08.014.

Dennis, K.J., Affek, H.P., Passey, B.H., Schrag, D.P., and Eiler, J.M., 2011, Defining an absolute reference frame for 'clumped' isotope studies of CO2: Geochimica et Cosmochimica Acta, v. 75, p. 7117–7131, doi:10.1016/j.gca.2011.09.025.

Dorsey, R.J., and LaMaskin, T.A., 2007, Stratigraphic Record of Triassic-Jurassic Collisional Tectonics in the Blue Mountains Province, Northeastern Oregon: American Journal of Science, v. 307, p. 1167–1193, doi:10.2475/10.2007.03.

Dunham, R.J., 1962, Classification of carbonate rocks according to depositional texture: Memoir - American Association of Petroleum Geologists, p. 108–121, http://stats.lib.pdx.edu/proxy.php?url=http://search.ebscohost.com/login.aspx?direct=true&db=geh&AN=1962-012122&site=ehost-live.

Eiler, J.M., and Schauble, E., 2004, 18O13C16O in Earth's atmosphere: Geochimica et Cosmochimica Acta, v. 68, p. 4767–4777, doi:10.1016/j.gca.2004.05.035.

Flügel, E., 2010, Microfacies of Carbonate Rocks: Analysis, Interpretation, and Application: Springer, 984 p.

Follo, M.Ford., 1994, Sedimentology and Stratigraphy of the Martin Bridge Limestone and Hurwal Formation (Upper Triassic to Lower Jurrasic) from the Wallowa Terrane, Oregon, *in* Geology of the Blue Mountains Region of Oregon, Idaho, and Washington: Stratigraphy, Physiography, and Mineral Resources of the Blue Mountains Region, U.S. Geological Survey, 1439.

Garzione, C.N., Dettman, D.L., and Horton, B.K., 2004, Carbonate oxygen isotope paleoaltimetry: evaluating the effect of diagenesis on paleoelevation estimates for the Tibetan plateau: Palaeogeography, Palaeoclimatology, Palaeoecology, v. 212, p. 119–140, doi:10.1016/j.palaeo.2004.05.020.

Ghosh, P., Adkins, J., Affek, H., Balta, B., Guo, W., Schauble, E.A., Schrag, D., and Eiler, J.M., 2006, 13C–18O bonds in carbonate minerals: A new kind of paleothermometer: Geochimica et Cosmochimica Acta, v. 70, p. 1439–1456, doi:10.1016/j.gca.2005.11.014.

Hales, T.C., Abt, D.L., Humphreys, E.D., and Roering, J.J., 2005, A lithospheric instability origin for Columbia River flood basalts and Wallowa Mountains uplift in northeast Oregon: Nature, v. 438, p. 842–845, doi:10.1038/nature04313.

Harbert, W., Hillhouse, J., and Vallier, T., 1995, Paleomagnetism of the Permian Wallowa terrane: Implications for terrane migration and orogeny: Journal of Geophysical Research: Solid Earth, v. 100, p. 12573–12588, doi:10.1029/94JB02129.

He, B., Olack, G.A., and Colman, A.S., 2012, Pressure baseline correction and high-precision CO2 clumped-isotope (Δ47) measurements in bellows and micro-volume modes: Rapid Communications in Mass Spectrometry, v. 26, p. 2837–2853, doi:https://doi.org/10.1002/rcm.6436.

Hiatt, E., 2000, Links between Depositional and Diagenetic Processes in Basin Analysis: Porosity and Permeability Evolution in Sedimentary Rocks, *in* Kyser, K. ed., Fluids and Basin Evolution, Mineralogical Association of Canada, p. 63–92.

Hoefs, J., 2018, Stable Isotope Geochemistry: Springer International Publishing AG.

Huntington, K.W. et al., 2009, Methods and limitations of 'clumped' CO2 isotope (Δ47) analysis by gas-source isotope ratio mass spectrometry: Journal of Mass Spectrometry, v. 44, p. 1318–1329, doi:https://doi.org/10.1002/jms.1614.

Huntington, K.W., Budd, D.A., Wernicke, B.P., and Eiler, J.M., 2011, Use of clumped-isotope thermometry to constrain the crystallization temperature of diagenetic calcite: Journal of Sedimentary Research, v. 81, p. 656–669, doi:10.2110/jsr.2011.51.

Huntington, K.W., and Lechler, A.R., 2015, Carbonate clumped isotope thermometry in continental tectonics: Tectonophysics, v. 647–648, p. 1–20, doi:10.1016/j.tecto.2015.02.019.

James, N.P., and Jones, B., 2016, Origin of Carbonate Sedimentary Rocks: AGUWiley.

Johnson, K., Schwartz, J.J., Wooden, J.L., O'Driscoll, L.J., and Jeffcoat, C.R., 2011, The Wallowa Batholith; new Pb/U (SHRIMP-RG) ages place constraints on arc magmatism and crustal thickening in the Blue Mountains Province, NE Oregon: Abstracts with Programs - Geological Society of America, v. 43, p. 5–5, http://stats.lib.pdx.edu/proxy.php?url=http://search.ebscohost.com/login.aspx?direct=true&db=geh&AN=2012-006852&site=ehost-live.

Karlstrom, L., Murray, K.E., and Reiners, P.W., 2019, Bayesian Markov-Chain Monte Carlo Inversion of Low-Temperature Thermochronology Around Two 8 − 10 m Wide Columbia River Flood Basalt Dikes: Frontiers in Earth Science, v. 7, p. 90, doi:10.3389/feart.2019.00090.

Kim, S.-T., and O'Neil, J.R., 1997, Equilibrium and nonequilibrium oxygen isotope effects in synthetic carbonates: Geochimica et Cosmochimica Acta, v. 61, p. 3461–3475, doi:https://doi.org/10.1016/S0016-7037(97)00169-5.

LaMaskin, T.A., Dorsey, R.J., Vervoort, J.D., Schmitz, M.D., Tumpane, K.P., and Moore, N.O., 2015, Westward Growth of Laurentia by Pre–Late Jurassic Terrane Accretion, Eastern Oregon and Western Idaho, United States: The Journal of Geology, v. 123, p. 233–267, doi:10.1086/681724.

Loyd, S.J., Corsetti, F.A., Eagle, R.A., Hagadorn, J.W., Shen, Y., Zhang, X., Bonifacie, M., and Tripati, A.K., 2015, Evolution of Neoproterozoic Wonoka–Shuram Anomaly-aged carbonates: Evidence from clumped isotope paleothermometry: Precambrian Research, v. 264, p. 179–191, doi:10.1016/j.precamres.2015.04.010.

Martindale, R.C., Corsetti, F.A., Bottjer, D.J., and Senowbari-Daryan, B., 2012, MICROBIALITE FABRICS AND DIMINUTIVE SKELETAL BIOCONSTRUCTORS IN LOWER NORIAN SUMMIT POINT REEFS, OREGON, UNITED STATES: PALAIOS, v. 27, p. 489–508, doi:10.2110/palo.2012.p12-001r.

McRoberts, C.A., 1990, Systematic paleontology stratigraphic occurrence and paleoecology of halobiid bivalves from the Martin Bridge Formation (Upper Triassic) Wallowa Terrane Oregon: University of Montana.

Morriss, M.C., Karlstrom, L., Nasholds, M.W.M., and Wolff, J.A., 2020, The Chief Joseph dike swarm of the Columbia River flood basalts, and the legacy data set of William H. Taubeneck: Geosphere, v. 16, p. 1082–1106, doi:10.1130/GES02173.1.

Moura, R.L. et al., 2016, An extensive reef system at the Amazon River mouth: Science Advances, v. 2, p. e1501252, doi:10.1126/sciadv.1501252.

Neuzil, C.E., 1994, How permeable are clays and shales? Water Resources Research, v. 30, p. 145–150, doi:https://doi.org/10.1029/93WR02930.

Nolf, B.O., 1966, Structure and Stratigraphy of Part of the Northern Wallowa Mountains, Oregon [Ph.D Dissertation]: Princeton University, 196 p.

O'Neil, J.R., Clayton, R.N., and Mayeda, T.K., 1969, Oxygen Isotope Fractionation in Divalent Metal Carbonates: The Journal of Chemical Physics, v. 51, p. 5547–5558, doi:10.1063/1.1671982.

Passey, B.H., and Henkes, G.A., 2012, Carbonate clumped isotope bond reordering and geospeedometry: Earth and Planetary Science Letters, v. 351–352, p. 223–236, doi:10.1016/j.epsl.2012.07.021.

Santrock, Jeffrey., Studley, S.A., and Hayes, J.M., 1985, Isotopic analyses based on the mass spectra of carbon dioxide: Analytical Chemistry, v. 57, p. 1444–1448, doi:10.1021/ac00284a060.

Schauer, A.J., Kelson, J., Saenger, C., and Huntington, K.W., 2016, Choice of 17O correction affects clumped isotope (Δ47) values of CO2 measured with mass spectrometry: Rapid Communications in Mass Spectrometry, v. 30, p. 2607–2616, doi:https://doi.org/10.1002/rcm.7743.

Siman-Tov, S., Affek, H.P., Matthews, A., Aharonov, E., and Reches, Z., 2016, Shear heating and clumped isotope reordering in carbonate faults: Earth and Planetary Science Letters, v. 445, p. 136–145, doi:10.1016/j.epsl.2016.03.041.

Stanley, G.D., McRoberts, C.A., and Whalen, M.T., 2008, Stratigraphy of the Triassic Martin Bridge Formation, Wallowa terrane: Stratigraphy and depositional setting, *in* Special Paper 442: The Terrane Puzzle: New Perspectives on Paleontology and Stratigraphy from the North American Cordillera, Geological Society of America, v. 442, p. 227–250, doi:10.1130/2008.442(12).

Stanley, G.D., and Senowbari-Daryan, B., 1986, Upper Triassic, Dachstein-Type, Reef Limestone from the Wallowa Mountains, Oregon: First Reported Occurrence in the United States: PALAIOS, v. 1, p. 172, doi:10.2307/3514511.

Swart, P.K., 2015, The geochemistry of carbonate diagenesis: The past, present and future: Sedimentology, v. 62, p. 1233–1304, doi:10.1111/sed.12205.

Swart, P.K., and Oehlert, A.M., 2018, Revised interpretations of stable C and O patterns in carbonate rocks resulting from meteoric diagenesis: Sedimentary Geology, v. 364, p. 14–23.

Walker, G.W., and MacLeod, N.S., 1991, Geologic map of Oregon: U.S. Geological Survey.

Whalen, M.T., 1988, Depositional history of an Upper Triassic drowned carbonate platform sequence: Wallowa terrane, Oregon and Idaho: Geological Society of America Bulletin, v. 100, p. 1097–1110, doi:10.1130/0016-7606(1988)100<1097:DHOAUT>2.3.CO;2.

Whalen, M.T., 1985, The carbonate petrology and paleoecology of Upper Triassic limestones of the Wallowa terrane Oregon and Idaho: University of Montana.

Wyld, S.J., and Wright, J.E., 2001, New evidence for Cretaceous strike-slip faulting in the United States Cordillera and implications for terrane-displacement, deformation patterns, and plutonism: American Journal of Science, v. 301, p. 150–181, http://stats.lib.pdx.edu/proxy.php?url=http://search.ebscohost.com/login.aspx?direct=true&db=geh&AN=2001-052717&site=ehost-live.

Yang, Y., and Aplin, A.C., 2010, A permeability–porosity relationship for mudstones: Marine and Petroleum Geology, v. 27, p. 1692–1697, doi:10.1016/j.marpetgeo.2009.07.001.

Zachos, J.C., Stott, L.D., and Lohmann, K.C., 1994, Evolution of early Cenozoic marine temperatures: Paleoceanography, v. 9, p. 353–387, doi:10.1029/93PA03266.

Appendix

Methods: Sample Locations

Table 4: Complete list of samples and locations. Note that samples 27-34 were not used in this study and as such are excluded from the dataset. EC = Eagle Creek, SP = Summit Point, ND = Not Described

Sample	Latitude	Longitude	Approximate Elevation (m)	Locality
MB19_01	44.9438	-117.33366	1062	EC
MB19_02	44.9438	-117.33366	1065	EC
MB19_03	44.9438	-117.33366	1060	EC
MB19_04	44.9438	-117.33366	1062	EC
MB19_05	44.9438	-117.33366	1065	EC
MB19_06	44.95131	-117.32373	1177	EC
MB19_07	44.95131	-117.32373	1177	EC
MB19_08	44.95358	-117.3229	1160	EC
MB19_09	44.98519	-117.24553	2091	SP
MB19_10	45.00578	-117.42946	1287	ND
MB19_11	45.00578	-117.42946	1287	ND
MB19_12	45.00578	-117.42946	1287	ND
MB19_13	45.00999	-117.35167	1287	ND
MB19_14	45.01133	-117.34971	1287	ND
MB19_15	44.98007	-117.24198	2005	SP
MB19_16	44.98262	-117.24439	2058	SP
MB19_17	44.97474	-117.2461	1747	SP
MB19_18	44.97474	-117.2461	1747	SP
MB19_19	44.97474	-117.2461	1747	SP
MB19_20	44.9445	-117.33228	1075	EC
MB19_21	44.9445	-117.33228	1075	EC
MB19_22	44.97959	-117.24852	1874	SP
MB19_23	44.97948	-117.24831	1883	SP
MB19_24	44.97922	-117.24715	1914	SP
MB19_25	44.97858	-117.24582	1894	SP
MB19_26	44.97858	-117.24582	1894	SP
MB19_35	44.9438	-117.33366	1060	EC
MB19_36	44.9438	-117.33366	1071	EC
MB19_37	44.9438	-117.33366	1071	EC
MB19_38	44.9445	-117.33228	1075	EC
MB19_39	44.97534	-117.24607	1780	SP
MB19_40	44.97474	-117.2461	1747	SP

MB19_41	44.97474	-117.2461	1748	SP
MB19_42	44.97474	-117.2461	1747	SP
MB19_43	44.98017	-117.24253	2008	SP
MB19_44	44.98262	-117.24439	2061	SP
MB19_45	44.98414	-117.2445	2088	SP
MB19_46	44.98414	-117.2445	2088	SP
MB19_47	44.98414	-117.2445	2088	SP

Methods: Δ_{47}

Carbonate clumped isotope analysis starts when carbonate samples (6-8 mg) are digested in a common bath of phosphoric acid (specific gravity 1.9-1.95) held at 90° C for 10 minutes. The evolved CO_2 is cryogenically separated from water on an automated nickel / stainless steel vacuum line using an ethanol-dry ice slush trap, isolated in a liquid N_2 trap, and passed through a Porapak Q trap (50/80 mesh, 122 cm long, 6.35 mm OD) held at -20 °C. The CO_2 is transferred through the Porapak Q trap using helium as the carrier gas with a flow rate of ~35 mL / min for a total transfer time of 20 minutes then isolated cryogenically and transferred into a Pyrex break seal. Every 5-8 carbonate sample unknowns, a solid carbonate standard (C64, C2, coral, or ETH 1-4) or CO_2 reference frame gas is purified on the vacuum line and transferred into a Pyrex break seal. The reference frame gases were created by equilibrating CO_2 that originated from corn fermentation or fossil fuel combustion in Pyrex break seals with South Pole ice core water, local tap water, or evaporatively-enriched water (such that the δ^{47} range is approximately 80 ‰) held at 4° C and 60° C, or by heating CO_2 in quartz break seals in a box furnace at 1000 °C. Break seals containing CO_2 purified on the vacuum line are loaded into an automated 10-port tube cracker inlet system on a Thermo MAT 253 configured to measure mass / charge (*m/z*) 44-

49, inclusive. To start each sample analysis, sample bellows are fully expanded and evacuated. Sample gas is expanded into the sample bellows and pressure is measured. Following sample gas filling, evacuated reference bellows at 100 % expansion is filled to a pressure equal to that measured in the sample bellows with UW 'fermented corn' reference CO_2 ($\delta^{13}C$ VPDB = -10.2‰, $\delta^{18}O$ VPDB = -6.0‰; values calibrated by NBS-19 international carbonate standard). Following bellow fill, the *m/z* - 45 signal is used for peak centering and bellows are compressed for pressure adjustment that produced a *m/z* 44 signal of 16 V (equivalent to ~ 2500 mV for *m/z* 47). Pressure baseline (PBL) is automatically measured similar to the method of (He et al., 2012) with the measurement made 0.08 kV left of peak center. Sample CO_2 *m/z* 44-49 is measured against reference CO_2 for 6 acquisitions of 15 sample-reference comparison cycles with 26-second integration times. Masses 44-46 are measured with standard amplification ($3x10^8$, $3x10^{10}$, $1x10^{11}$, respectively); masses 47-49 are measured with $1x10^{12}$ Ω amplification. At the end of each 6-acquisition sample measurement, water backgrounds are measured by peak centering on the mass-45 faraday collector and measuring *m/z* 18 of both sample and reference. Δ_{47} values are calculated using established methods (Santrock et al., 1985; Eiler and Schauble, 2004; Huntington et al., 2009; Brand et al., 2010; Schauer et al., 2016; Daëron et al., 2016) and are corrected to the carbon dioxide equilibrium scale (CDES) of (Dennis et al., 2011) using CO_2 equilibrated with a suite of waters and at three temperatures (4 °C, 60 °C, 1000 °C). We also use a suite of internal carbonate standards as well as the four ETH carbonates to track precision and accuracy in Δ_{47}, $\delta^{13}C$, and $\delta^{18}O$.

Methods: $\Delta^{18}O_w$ Calculation

I calculated $\Delta^{18}O_w$ values using the calcite-water fractionation equation of O'Neil et al. (1969) (Equation 4). I chose this equation over the updated equation of Kim and O'Neil (1997) because it is derived for temperatures ranging from 0 to 500°C, whereas the Kim and O'Neil equation is derived for lower temperatures (10 - 40°C).

$$1000 \ln \alpha = 2.78(10^6 T^{-2}) - 3.39 \quad (4)$$

$$R_w = \frac{0.0020672\left(\frac{\delta^{18}O_{carb}}{10^3} + 1\right)}{\alpha} \quad (5)$$

$$\delta^{18}O_w = 10^3\left(\frac{R_w}{0.0020052} - 1\right) \quad (6)$$

Where *T* is the temperature in Kelvin, as given by clumped isotope data.

Methods: Water-Rock Modeling

Table 5: Model input parameters for Figure 17 in the main text. Note that C_o and F are dictated by the W/R ratio.

Input Parameter	Value
C_s (mol)	0.48
C_f (mol)	0.89
$\delta_{o,s}$ (‰, VSMOW)	31
$\delta_{o,f}$ (‰, VSMOW)	-10, 0, 10
W/R range	0.01 to 1
C_o range (mol)	0.48 to 0.69
F range	0.01 to 0.5
Temperature range (°C)	0 to 350
α range	1.004 – 1.034

Results: Paleo-Meteoric Water Calculations

I calculated paleo-meteoric water using the equation of Bowen and Wilkenson (2002), which allows calculation of $\delta^{18}O_{ppt}$ at a given latitude and elevation (Equation 7).

$$\delta^{18}O_{ppt} = -0.0051(|LAT|)^2 + 0.1805(|LAT|) - 0.002(ALT) - 5.247 \qquad (7)$$

Following Wyld and Wright's (2001) reconstruction of the Wallowa terrane's position in early Cretaceous time and Harbert et al.'s (1995) reconstruction of the Wallowa terrane's position in mid-late Triassic time, I used the following input parameters:

LAT = 41, 24

ALT = 0